Rapid and Inducible Mislocalization of Endogenous TDP43 in a Novel Human Model of Amyotrophic Lateral Sclerosis

Johanna Ganssauge[1,2], Sophie Hawkins[*1,3], Seema C. Namboori[*1,3], Szi Kay Leung[3], Jonathan Mill[3], Akshay Bhinge[1,3#]

1. Living Systems Institute, University of Exeter, EX4 4QD, UK
2. Biosciences, University of Exeter, EX4 4QD, UK
3. Clinical and Biomedical Sciences, University of Exeter, EX4 7BS, UK

* Indicates these authors contributed equally

# indicates corresponding author

Keywords: ALS, TDP43, proteinopathy, iPSC, splicing, microRNA, mislocalization, aggregation.

Abstract

Transactive response DNA binding protein 43 kDa (TDP43) proteinopathy, characterized by the mislocalization and aggregation of TDP43, is a hallmark of several neurodegenerative diseases including Amyotrophic Lateral Sclerosis (ALS). In this study, we describe the development of a new model of TDP43 proteinopathy using human induced pluripotent stem cell (iPSC)-derived neurons. Utilizing a genome engineering approach, we induced the mislocalization of endogenous TDP43 from the nucleus to the cytoplasm without mutating the TDP43 gene or using chemical stressors. Our model successfully recapitulates key early and late pathological features of TDP43 proteinopathy, including neuronal loss, reduced neurite complexity, and cytoplasmic accumulation and aggregation of TDP43. Concurrently, the loss of nuclear TDP43 leads to splicing defects, while its cytoplasmic gain adversely affects microRNA expression. Strikingly, our observations suggest that TDP43 is capable of sustaining its own mislocalization, thereby perpetuating and further aggravating the proteinopathy. This innovative model provides a valuable tool for the in-depth investigation of the consequences of TDP43 proteinopathy. It offers a clinically relevant platform that will accelerate identification of potential therapeutic targets for the treatment of TDP43-associated neurodegenerative diseases including sporadic ALS.

Introduction

Amyotrophic Lateral Sclerosis (ALS) is a devastating neurodegenerative disorder characterised by the relentless degeneration of motor neurons (MNs) in both the brain and spinal cord (R. H. Brown and Al-Chalabi 2017). This degeneration precipitates a cascade of symptoms including muscle weakness, atrophy, and paralysis, eventually leading to

respiratory failure and death typically within three to five years after the onset of symptoms (Hardiman et al. 2017).

A hallmark of ALS pathology is the aberrant behavior of the TAR DNA-binding protein 43 (hereafter TDP43). In ALS patients, TDP43, which normally resides in the nucleus, becomes mislocalized, forming aggregates in the cytoplasm of neurons and glial cells (Neumann et al. 2006). This phenomenon, termed TDP43 proteinopathy, is implicated in the majority of ALS cases and is considered a central player in the disease's pathogenesis (S.-C. Ling, Polymenidou, and Cleveland 2013). TDP43 proteinopathy is a common feature in multiple age-associated neurodegenerative diseases including ALS, Limbic-predominant age-related TDP43 encephalopathy (LATE), frontotemporal dementia (FTD) and Alzheimer's disease (AD) (de Boer et al. 2020). TDP43 (encoded by *TARDBP*) is an RNA-binding protein that plays a critical role in RNA metabolism, encompassing RNA splicing (Donde et al. 2019; Polymenidou et al. 2011; Arnold 2012; J. P. Ling et al. 2015), stabilization (Sidibé et al. 2021), and transport (Nagano et al. 2020; Chu et al. 2019) thus ensuring proper neuronal function (Gimenez et al. 2023). For example, recent studies have demonstrated cryptic exon (CE) inclusion triggered by loss of nuclear TDP43 (J. P. Ling et al. 2015), especially in transcripts of important neuronal genes *UNC13A (*Brown et al. 2022; Ma et al. 2022*)* and *STMN2* (Klim et al. 2019; Melamed et al. 2019). Additionally, TDP43 associates with the microRNA biogenesis machinery and affects microRNA expression (Buratti et al. 2010; Kawahara and Mieda-Sato 2012; Paez-Colasante et al. 2020). Accordingly, widespread dysregulation of microRNA levels have been reported in spinal tissue obtained post-mortem from sporadic ALS cases (Reichenstein et al. 2019; Emde et al. 2015; Figueroa-Romero et al. 2016; Gagliardi et al. 2019).

Current cellular models aimed at investigating TDP43 mislocalization involve mutating the TDP43 nuclear-localization signal, using mutant versions identified in familial ALS patients, or the use of pharmacological agents to induce stress (Barmada et al. 2010; Zuo et al. 2021; Ziff et al. 2023; Walker et al. 2015). Despite the insights gained from these models, they harbor inherent limitations. Overexpression may not represent physiological conditions, TDP43 is found to be mutated in <0.5% of all ALS cases, and pharmacological induction might induce events unrelated to the disease. Further, CEs identified in ALS/FTD cases are poorly conserved beyond primates, making it challenging to investigate the contribution of splicing defects to ALS pathophysiology using animal models (Baughn et al. 2023). Human induced pluripotent technology (iPSCs) offers a powerful platform that addresses some of these issues with animal models, enabling the development of human models of ALS *in vitro* (Giacomelli et al. 2022). A recent study employed sporadic ALS (spALS) spinal cord extracts

to induce TDP43 proteinopathy in iPSC-derived MNs (Smethurst et al. 2020). However, the model's utility is limited by the small percentage of neurons showing TDP43 pathology and the difficulty in producing spALS spinal extracts consistently and in large quantities.

In this study, we present an innovative human model of TDP43 proteinopathy that allows us to trigger cytoplasmic mislocalization of endogenous non-mutated TDP43 on demand in healthy control iPSC-MNs at scale (Fig. 1A). This technological advancement offers an unprecedented level of insight into TDP43 proteinopathy and its role in ALS.

Results and Discussion

We fused green fluorescent protein (GFP) to the C-terminus of *TARDBP* in its endogenous locus in healthy control iPSCs using CRISPR-Cas9 genome editing (Fig. 1A) and selected iPSC clones with a homozygous knock-in (Supplementary Fig. 1A). We initially ascertained that the integration of GFP did not adversely impact the differentiation of iPSCs into motor neurons (MNs). To this end, iPSCs engineered with TDP43-GFP were subjected to differentiation directed towards the MN lineage, employing protocols we had established in previous studies (Namboori et al. 2021, Hawkins et al. 2022). Based on the expression of established MN markers - ISLET1 (ISL1) and neurofilament-M (NF-M) - we confirmed that the edited iPSCs (with GFP integration) efficiently differentiated into MNs (Supplementary Fig. 1B). Moreover, the TDP43-GFP knock-in MNs did not show significantly altered expression levels of *TARDBP*, *UNC13A* and *STMN2*, nor did it cause any upregulation of cryptic transcripts in *STMN2* or *UNC13A* (Supplementary Fig. 1C). Overall, these results support the premise that the GFP knock-in had no detrimental effects on the iPSCs' ability to differentiate into MNs or TDP43 function.

These engineered iPSCs, hereafter called TDP43-GFP iPSCs, were differentiated into MNs (called TDP43-GFP MNs) where ~80% of the cells in culture immunostained positive for ISL1. We expressed an anti-GFP nanobody (12kDa) using adeno-associated viruses (AAVs) in the TDP43-GFP MNs. Expression of the nanobody (deemed the control nanobody) did not affect TDP43 localization from the nucleus (Fig. 1B). We engineered the nanobody with a nuclear export signal (NES). Expression of the NES-nanobody in the TDP43-GFP neurons caused relocation of the fusion protein to the cytoplasm with a concomitant loss in the nucleus (Fig. 1B,C, Supplementary Fig. 2A). We observed that TDP43 mislocalization leads to reduced dendrite complexity and neuronal soma swelling (Fig. 1D, Supplementary Fig. 2A) and an increase in cleaved caspase-3 activation (Fig. 1D, Supplementary Fig. 2B), which is an indicator of apoptosis. We confirmed that expression of the nanobodies in unedited iPSCs did not lead to apoptosis activation or dendrite defects, confirming that the observed phenotypes are due to TDP43 mislocalization (Supplementary Fig. 2C).

Additionally, we observed TDP43 puncta reminiscent of aggregates in the cytoplasm of MNs displaying mislocalized TDP43 that varied in size and number across individual neurons (Fig. 1E,F, Supplementary Fig. 1D).

Having demonstrated that our model can recapitulate cellular features observed in sporadic ALS, we next explored the molecular consequences triggered by TDP43 proteinopathy. Previous studies have highlighted the prevalence of alternative splicing defects affecting transcripts expressed from *UNC13A* and *STMN2* in ALS (A.-L. Brown et al. 2022; Ma et al. 2022; Klim et al. 2019; Melamed et al. 2019). These splicing defects are considered hallmarks in the progression of the disease. Given the significance of this phenomenon, we sought to ascertain if MNs expressing the NES nanobody exhibit these characteristic splicing defects. We performed RT-qPCR analysis on motor neurons that expressed the control or NES nanobody. The results strikingly mirrored the commonly observed ALS profile, showing inclusion of cryptic exons in both *UNC13A* and *STMN2* and a reduction in the abundance of canonical transcripts (Supplementary Fig. 2D). This demonstrated that our model proficiently recapitulates the critical molecular features observed in sporadic ALS.

Next, we ventured to explore the molecular consequences triggered by TDP43 proteinopathy across the whole transcriptome. We performed transcriptomic analysis on day 40 TDP43-GFP MNs to assess changes in the gene expression profiles due to TDP43 mislocalization. Principal component analysis (PCA) demonstrated that the primary axis of variance (90%) is related to the expression of the control and NES nanobody while the much smaller 2nd PC component related to the two clones (Fig. 2A). Subsequently, we conducted a differential gene expression analysis using DESeq2 and visualized the results via a volcano plot. Our analysis revealed differential expression of hundreds of genes with a fold change of ≥ 2 and false discovery rate (FDR) < 0.01, suggesting a profound impact of TDP43 dysfunction on the transcriptome of MNs (Fig. 2B). Gene ontology (GO) analysis of the differentially expressed genes highlighted a significant enrichment of pathways related to synaptic dysfunction and cytoskeletal defects in axons and dendrites amongst downregulated genes (Fig. 2C). This finding is of considerable relevance to ALS pathogenesis, as neurons affected by ALS often exhibit impairments in these functions. In contrast, upregulated genes were enriched for GO terms related to RNA processing including the nonsense mediated decay (Fig. 2C).

Given that alternative splicing (AS) defects are a hallmark of sporadic ALS, we utilized Leafcutter (Li et al. 2018) to analyze potential alternative splicing in MNs caused by TDP43 mislocalization. Our analysis identified alterations in the splicing of 175 genes, including

UNC13A and *STMN2* (ΔPSI > 0.1, adjusted p-value < 0.01). To gain functional insights into these splicing defects, we performed pathway enrichment analysis on affected genes, identifying a significant enrichment of terms related to synaptic development (FDR < 0.01). Furthermore, to gain mechanistic understanding of the role of TDP43 in the observed splicing defects, we compared the splicing results with TDP43 eCLIP data generated in the SH-SY5Y neuroblastoma cell line (Tam et al. 2019). Interestingly, only 35% of the splicing changes were proximal to a TDP43 binding site (Supplementary Fig. 3 and 4). This suggests that the loss of TDP43 from the nucleus may be responsible for a subset of the observed splicing defects but not all. This indicates the possibility of additional indirect underlying mechanisms that may include dysregulation of other RBPs or epitranscriptomic modifications of the RNA targets (McMillan et al. 2023). To gain deeper insights into the observed splicing patterns due to TDP43 mislocalization, we employed the Oxford Nanopore Technologies (ONT) long-read sequencing platform to generate RNA-seq data at the isoform level. Our investigation predominantly focused on *STMN2* due to its significance in ALS and a substantial number of reads (>100) mapping to this gene. Employing our FICLE pipeline (Leung et al. 2023), we identified a total of 476 isoforms related to *STMN2*. Out of these, 17 isoforms were congruent with the exonic structure of known reference isoforms. Notably, 40 isoforms, accounting for 8.4% of the total, were characterized by a cryptic exon (CE) starting at chr8:80529057 (Supplementary Fig. 5A). These isoforms with the CE were exclusively expressed in TDP43-GFP MNs that expressed the NES nanobody. Furthermore, the ONT data revealed that *STMN2* isoforms exhibit variable CE lengths, with different CE lengths corresponding to widely varying expression levels of the parent isoform (Supplementary Fig. 5B). Importantly, the isoforms containing the CE were predominantly short, truncated, and predicted to be non-protein coding. Surprisingly, four of these CE-containing isoforms manifested a novel exon, 114 bp in length, positioned upstream of the CE (Supplementary Fig. 5A). Our findings reveal a potentially significant variability in the splicing alterations induced by TDP43 proteinopathies, even within a single gene. This highlights the power of using long-read sequencing as a method for uncovering nuanced changes in splicing alterations in neurodegenerative diseases.

We compared our splicing results with publicly available transcriptomic data generated from cortical neuronal nuclei with or without TDP43 purified from ALS patient tissue post-mortem. At a stringent FDR threshold of 0.01 and ΔPSI > 0.1, we detected 90 genes as alternatively spliced in nuclei that showed a loss of TDP43 using Leafcutter. Thirty-four out of these 90 genes were also detected in our iPSC model (Fig. 2D), indicating strong concordance between the iPSC model and patient data, despite the differences in sample origin and neuronal subtype. Importantly, all 34 genes displayed an identical splicing event. To

evaluate whether the observed splicing changes were due to nuclear loss of TDP43, we compared our splicing results with transcriptomic data generated in iPSC-derived MNs and iNeurons after TDP43 knockdown (KD) (Fig. 2E, 2F). In accordance with the model that nuclear loss of TDP43 drives splicing changes, we observed a significant overlap between splicing defects due to a global loss of TDP43 and our mislocalization model (Fig. 2E, 2F). However, a number of genes that displayed splicing changes due to TDP43 mislocalization were not affected by TDP43 KD in either dataset (143 genes for the GSE121569 and 79 genes for the PRJEB42763 dataset). This indicates that nuclear loss of TDP43 alone cannot entirely explain the widespread defects in AS.

To generate a robust list of AS events associated with TDP43 pathology, we compared genes identified in our RNA-seq data with those from ALS/FTD post-mortem tissue. We applied an adjusted p-value threshold of 0.01 and a ΔPSI > 0.1. Additionally, to ensure further confidence in the identified changes, we required that each event be statistically significant at a stringent p-value threshold of 1e-4 in at least one dataset. Our analysis identified 12 genes, including *STMN2* and *UNC13A*, that we further investigated using RT-qPCR. This confirmed AS events in all the genes identified, where 9/12 genes displayed a decrease in expression of their canonical transcript levels (Fig. 2G). Further, most of these genes also displayed AS changes due to TDP43 KD in iPSC-MNs, although the extent of these changes for a subset of the genes tested was less dramatic (Supplementary Fig. 6).

A key drawback with earlier TDP43 models was the inability to characterize early changes after TDP43 mislocalization in neurons. To enable inducible control of TDP43 cytoplasmic localization in our model, we expressed the nanobody under a doxycycline-inducible promoter, and the entire circuit was knocked into the *AAVS1* locus in the E8 homozygous TDP43-GFP iPSCs. We called these iPSCs TDP43-GFP-CTRL or TDP43-GFP-NES iPSCs (Fig. 3A). We first confirmed that we could induce TDP43 mislocalization in the TDP43-GFP-CTRL/NES iPSC-derived MNs using doxycycline (Dox). Dox (1 µg/ml) triggered significant TDP43 mislocalization in the TDP43-GFP-NES MNs, while the TDP43-GFP-CTRL MNs, and the TDP43-GFP-NES MNs without Dox, maintained nuclear TDP43 (Fig. 3B). Further, we observed cytoplasmic TDP43 puncta in the NES line (Fig. 3C), and a significant increase in phosphorylated TDP43 without a change in the total TDP43 protein levels upon mislocalization (Fig. 3D, 3E). We noted that the TDP43 mislocalization alone did not induce significant levels of G3BP1+ stress granules (SG) (Supplementary Fig. 7). When treated with sodium arsenite, both control and NES MNs displayed cytoplasmic SG (Supplementary Fig. 7). However, in NES MNs treated with SA, only a subset of cytoplasmic TDP43 puncta co-localized with G3BP1+ stress granules (Supplementary Fig. 7).

To detect early changes in expression and splicing post-TDP43 mislocalization, we performed a time-course analysis of TDP43-GFP-NES at 4-, 8-, 12-, and 24-hours post-Dox addition. Notably, we observed TDP43 mislocalization as early as eight hours after Dox treatment (Fig. 4A), which was accompanied by significant AS errors in all 12 genes (Fig. 4B). This suggests that dysfunctional AS could be one of the incipient molecular events in ALS pathogenesis due to TDP43 mislocalization. Transcriptomic analysis of day 40 MNs uncovered splicing defects including cryptic exon inclusions and isoform switching in 494 genes (adjusted p-value < 0.01 and $\Delta PSI > 0.1$), with significant enrichment in pathways related to synaptic function and the cytoskeleton (Supplementary Fig. 9).

A significant area of research in the field of ALS involves pinpointing the upstream triggers responsible for causing the mislocalization of TDP43. The underlying premise of these investigations is that eliminating the trigger may potentially reverse the mislocalization of TDP43. However, it remains to be confirmed whether this hypothesis holds true. We wanted to ascertain whether TDP43, once mislocalized, self-perpetuates in its mislocalized state even after the initial trigger has been removed.

To investigate whether TDP43 mislocalization is self-perpetuating, we tagged both the control and NES nanobody with a V5 tag to track their expression. These were introduced into TDP43-GFP MNs using lentiviruses under a doxycycline (Dox)-inducible promoter. We induced TDP43 mislocalization by adding Dox to iPSC-derived MNs at day 20. After five days (day 25), Dox was withdrawn, and neurons were harvested 21 days later (day 46). As a benchmark of successful mislocalization, cultures were continuously treated with Dox (Constant Dox), while neurons expressing the control nanobody served as controls, displaying nuclear TDP43. TDP43 localization was assessed using immunofluorescence microscopy, and nanobody expression was evaluated via V5 immunostaining.

As expected, neurons in the Constant Dox NES condition exhibited significant TDP43 mislocalization, while TDP43 remained nuclear in the Constant Dox control MNs, confirming the specificity of Dox-induced mislocalization (Fig. 5A, B). Following Dox withdrawal, TDP43 localization was largely restored to the nucleus. However, a subset of neurons retained cytoplasmic TDP43 even after 21 days (Fig. 5A). Super-resolution microscopy further revealed persistent cytoplasmic TDP43 in these neurons, despite near undetectable nanobody expression (Fig. 5C), suggesting that in some cells, TDP43 mislocalization may become self-sustaining. Our data indicates that removal of the initial trigger maybe insufficient to completely reverse TDP43 once it has been mislocalized.

Finally, since TDP43 is involved in microRNA biogenesis, we sought to analyze changes in the microRNA profiles associated with TDP43 mislocalization. For this purpose, we carried out small RNA sequencing on day 40 MNs after triggering TDP43 mislocalization at day 20 by the addition of doxycycline. Our analysis revealed a striking alteration in the landscape of microRNA expression as a result of TDP43 mislocalization. Principal component analysis (PCA) demonstrated distinct separation of the control and mislocalized samples (PC1 77%), emphasizing the profound impact of TDP43 mislocalization on microRNA profile (Supplementary Fig. 10A).

Around 150 microRNAs were found to be significantly altered (FDR < 0.01 and fold change ≥ 1.5) upon TDP43 mislocalization. Our data captured downregulation of the microRNAs miR-218, and miR-9, which have previously been shown to be downregulated in ALS MNs (Reichenstein et al. 2019) (Zhang et al. 2013). Interestingly, these changes were not unidirectional; almost equal numbers of microRNAs were upregulated or downregulated (Supplementary Fig. 10B). The results of this study indicate that TDP43 mislocalization leads to global dysregulation of microRNA expression in iPSC-derived MNs. However, it is noteworthy that our observations contrast with those found in postmortem tissue studies, where all differentially expressed microRNAs were reported to be downregulated. This divergence in findings may suggest that the uniform downregulation observed in postmortem tissues could be attributed to changes that are triggered by end-stage dying neurons, which might not represent the whole spectrum of molecular alterations especially early in the disease progression.

We wanted to evaluate whether alterations in microRNA expression profiles induced by TDP43 mislocalization are congruent with the changes caused by TDP43 knockdown. For this investigation, small RNA sequencing was utilized to assess microRNA expression in motor neurons (MNs) at day 30 following the knockdown of TDP43 using shRNAs. Again, principal component analysis revealed a distinct separation between all control and TDP43 knockdown samples, indicating a clear impact of TDP43 knockdown on microRNA expression profiles (Supplementary Fig. 10C). However, a striking contrast was observed in the number of microRNAs affected by TDP43 knockdown as compared to TDP43 mislocalization. Specifically, in the case of TDP43 knockdown, only one microRNA (miR-1249-3p) exhibited a significant change (FDR < 0.01 and a fold change of 1.5) (Supplementary Fig. 10D). This is in stark contrast to the observations made when TDP43 was mislocalized, where over 150 microRNAs displayed altered expression. To avoid setting thresholds in our comparisons, we first ranked the microRNAs impacted by TDP43 knockdown based on their fold changes. Subsequently, we utilized gene set enrichment

analysis (GSEA) to determine if the microRNAs disrupted by TDP43 mislocalization significantly coincided with our knockdown data. We observed a substantial overlap between microRNAs that were downregulated due to TDP43 mislocalization and those downregulated following TDP43 knockdown (Supplementary Fig. 10E). However, we did not observe a significant overlap for microRNAs that were upregulated in both scenarios (Supplementary Fig. 10F). Our data suggests that mislocalized TDP43 selectively affects the expression of a subset of microRNAs. Additionally, these observations highlight the possibility that the nuclear loss and cytoplasmic gain of TDP43 induce distinct molecular alterations within motor neurons that converge to hasten neuronal dysfunction and demise.

However, we acknowledge that another explanation for the observed differences between microRNA dysregulation and splicing could be the extent of nuclear TDP43 loss. Our knockdown approach resulted in a 60% reduction in TDP43 transcripts. Though this was sufficient to cause splicing defects, it is possible that microRNA dysregulation might be more resilient to TDP43 loss as compared to splicing changes.

Limitations of the study

We could not confirm whether the observed cytoplasmic puncta are true aggregates. Attempts to immunostain neurons for phosphorylated TDP43 were unsuccessful. Using the Cosmo Bio antibody (TIP-PTD-M01A), we detected no signal, while the Proteintech antibody (22309-1-AP) showed nuclear phosphorylation even in control neurons. To address this, we performed western blot analysis with the Cosmo Bio antibody, which clearly detected hyperphosphorylated TDP43 in whole-cell lysates (Fig. 3D, E). Given these results, we refer to these structures as "puncta" rather than aggregates.

TDP43 undergoes alternative splicing within exon 6 in response to induced hyperexcitability in iPSC-derived iNeurons, generating truncated proteins. These isoforms are detected in lumbar motor neurons; however, their levels remained unchanged between ALS patient and healthy tissue (Weskamp et al. 2020). Since our GFP tag is positioned on the C-terminus, our system cannot manipulate these truncated fragments as the tag is lost in these isoforms. But these isoforms, if present, should be detectable using the Proteintech antibody against total TDP43, which recognizes N-terminal TDP43 epitopes. However, western blot analysis, even 20 days after inducing TDP43 mislocalization, showed no truncated fragments. This suggests that TDP43 mislocalization alone is insufficient to generate significant levels of truncated isoforms.

Summary

In summary, our unique iPSC model of TDP43 proteinopathy offers an unprecedented access to investigate cellular and molecular events in human neurons in a temporal fashion downstream of TDP43 mislocalization. This model faithfully captures the neuronal loss and cytoplasmic accumulation characteristics of TDP43 proteinopathies. Beyond neurons, our model paves the way for inquiries into the roles of non-neuronal cells, such as oligodendrocytes and astrocytes, which also exhibit TDP43 proteinopathy, in contributing to neuronal dysfunction in a cell non-autonomous manner (Barton et al. 2021; James et al. 2022; Smethurst et al. 2020; Licht-Murava et al. 2023). We expect this model to not only enhance our understanding of ALS but also other TDP43 proteinopathies and accelerate efforts into developing therapies against these devastating neurodegenerative diseases.

Acknowledgements

We would like to thank Aaron Jeffries and the University of Exeter Sequencing Center for the Illumina and Oxford Nanopore Technologies long read sequencing. Thanks to Jessica Board for her help with the TDP43 shRNAs. Thanks to Bradely Dyer and Corin Liddle from the Exeter Bioimaging Center for their help with the Zeiss LSM880 Airyscan imaging. This study was funded by an MNDA Pilot award and an MRC New Investigator Research Grant to A.B.. This study was supported by the National Institute for Health and Care Research Exeter Biomedical Research Centre. The views expressed are those of the author(s) and not necessarily those of the NIHR or the Department of Health and Social Care.

Availability of data and materials: The RNA-seq data is available on the Gene Expression Omnibus database with the following accession IDs: GSE290436, GSE290437, GSE290441. All qPCR and western blot analysis data have been included in the supplementary excel file.

Competing interests: The authors declare that they have no competing interests.

Author Contributions: JG performed the experiments and analyzed and interpreted all data. SH analyzed the transcriptomics data. SN performed experiments pertaining to developing the TDP43-GFP iPSC lines and the phenotyping. SZL and JM analyzed and interpreted the ONT long read data. AB conceived and funded the study, and performed experiments related to developing the model and analyzing the transcriptomic data.

Materials and Methods

Genome Editing

CRISPR-Cas9 GFP knock-in into the TDP43 C-terminus was performed on healthy iPSC lines (GM23280A, Coriell Institute for Medical Research). The iPSCs were maintained as colonies on Matrigel (Corning) in StemFlex (StemCell Technologies).

The eGFP donor plasmid was designed to add a 13 amino acid linker between the TDP43 2nd last codon and eGFP sequence as described previously (Barmada et al. 2010) and carried 400 bp homology arms on the 5' and 3' end of the TDP43 stop codon. For genome editing, iPSCs were transfected with the eGFP donor plasmid and sgRNA targeting TDP43 C-terminus (GAATGTAGACAGTGGGGTTG).

Knock-in of GFP was confirmed via PCR and the sequence was validated using Sanger sequencing. Two independently edited homozygous clones ("E5" and "E8") were selected. The nanobody sequence was obtained from Addgene plasmid 136619 (a kind gift from Kai Johnsson (Farrants et al. 2020) and synthesized as a gBlock from IDT. The NES sequence from the MAPKK gene MNLVDLQKKLEELELDEQQ was added onto the nanobody sequence to create the NES nanobody at its C-terminus using PCR primers. An unrelated sequence IDEAAKELPDANA was used to create the control nanobody.

For the TDP43-GFP-NES and TDP43-GFP-CTRL lines, the donor vector was created by cloning in the NES or control nanobody sequences into Addgene plasmid 52343 (a kind gift from Su-Chun Zhang (Qian et al. 2014). Homozygous TDP43-GFP iPSCs derived from clone E8 were transfected with the donor vectors, and a sgRNA targeting the human *AAVS1* locus (Addgene 126582, a kind gift from Michael Guertin (Sathyan et al. 2019)). The nanobody sequence was PCR amplified from Addgene. Edited cells were selected with puromycin (0.5 µg/ml) treatment for a minimum of 4 days.

Cell Culture

Motor neurons were generated from iPSCs as described previously (Namboori et al. 2021, Hawkins et al. 2022). Briefly, iPSCs were plated onto matrigel and differentiated by treatment with neuronal differentiation media (DMEM/F12: Neurobasal in a 1:1 ratio, HEPES 10 mM, N2 supplement 1%, B27 supplement 1%, L-glutamine 1%, ascorbic acid 5 µM) supplemented with SB431542 (40 µM), CHIR9921 (3 µM) and LDN98312 (0.2 µM) from day 0 until day 4. Cells were caudalized by treatment with 0.1 µM retinoic acid starting at day 2 and ventralized with 1 µM purmorphamine starting at day 4 and continued until day 10. At day 8, progenitors were replated onto poly-D-lysine/laminin coated wells and differentiated with 10 µM DAPT for 3 days. Undifferentiated cells were removed with a pulse of 10 µg/ml mitomycin-C for 1 hour at day 14. Motor neurons were subsequently maintained in N2B27

media supplemented with 10 ng/ml BDNF and GDNF, with half media changes occurring twice per week.

TDP43-GFP mislocalization was induced via transduction with AAVs expressing anti-GFP nanobodies. In our TDP43-GFP-NES/ CTRL cell line, TDP43-GFP mislocalisation was achieved via addition of 1 µg/mL doxycycline, which was replenished every 48 hours.

Immunocytochemistry

Cells were fixed in 4% paraformaldehyde for 20 minutes at room temperature (RT), followed by permeabilization in ice-cold methanol for 5 minutes. Blocking was performed in 1% BSA (in PBS) for 1 hour (RT) and primary antibodies (Supplementary Table 2) were incubated overnight at 4°C. Next day, wells were washed in PBS. Secondary antibodies (Molecular probes, 1:2,000) were incubated for 1-2 hours (RT), and nuclei were stained with Hoechst 33542 (1:1,000; Molecular Probes). All antibodies were diluted in blocking agent. Plates were imaged using ImageXpress® Pico (Molecular Devices). Super-resolution images were captured using the Zeiss LSM880 Confocal with Airyscan.

Phenotypic analysis

Image analysis was conducted using custom scripts in CellProfiler (Stirling et al. 2021). To ensure accurate dendritic complexity measurements, we discarded soma that displayed overlapping dendrites from different neurons to prevent confounding effects. For CC3 analysis, we chose soma that did not overlap and were separated by at least 10 pixels, as CC3 intensities were quantified specifically within the soma. This adjustment allowed for a larger number of cells to be included in the CC3 analysis compared to the morphological analysis.

RNA Sequencing and analysis

RNA was extracted using the QIAzol and the NEB Monarch RNA extraction kit and ribosomal RNA was depleted using the NEBNext rRNA depletion kit (NEB). Libraries for Illumina short-read sequencing were prepared using the NEBNext Ultra II RNA library kit (NEB) according to manufacturer instructions. Sequencing was performed at the Exeter sequencing centre using the NovaSeq platform. Reads were mapped to the human genome assembly hg19 using STAR (Dobin et al. 2013) and counts for each gene per sample were generated using the R package featureCounts (Liao, Smyth, and Shi 2014). Differential expression analysis was performed using DESeq2 (Love, Huber, and Anders 2014). Alternatively spliced transcripts were detected using Leafcutter (Li et al. 2018). Libraries for

long read ONT platform were prepared according to the manufacturer's instructions and sequenced on a PromethION sequencer at the Exeter sequencing centre. Reads were mapped to hg19 using minimap2 (Li 2018), isoform counts were generated using FLAIR (Tang et al. 2020), and transcript isoforms were analyzed using the FICLE pipeline (Leung et al. 2023). Small RNA sequencing was performed commercially through Macrogen and the fastq data was mapped and counts generated using the miRDeep2 package (Friedländer et al. 2008). Differential expression was performed using DESeq2.

RT-qPCR

Following lysis in QIAzol, total RNA was purified using the miRNeasy Micro Kit (Qiagen). A total of 500 ng RNA was used for the generation of cDNA using the High-capacity cDNA kit (ThermoFisher). The RT-qPCR was performed using the Promega® 2x Master Mix and the QuantStudio™ 6 (Applied Biosystems) for 40 cycles. Housekeeping genes *GAPDH, HPRT1*, and *RPL13* were used for normalization. Using the ΔΔCt method, fold changes were calculated per sample relative to their appropriate control. A maximum Ct value of 33 was selected for all samples. Significance testing was performed using the student's T-test. Primer sequences have been included in Supplementary Table 1.

Western Blotting

Motor neuron samples at D40 were lysed in ice-cold RIPA buffer supplemented with HALT™ protease phosphatase inhibitors. Lysates were centrifuged at 500 x g, for 10 minutes at 4°C to remove cellular debris. The supernatant was used as the total protein fraction. A total of 3 µg protein was separated by SDS-PAGE gel electrophoresis (Bio-Rad) and transferred to 0.2 µm nitrocellulose membrane (Amersham™ Protran™) for immunoblotting. Membranes were blocked for 1 hour at RT using the Intercept-T blocking buffer (Li-Cor). Primary antibodies (Supplementary Table 2) were incubated overnight at 4°C. Secondary antibodies were incubated for 1 hour at RT. All antibodies were diluted in Intercept-T with 0.2% Tween-20 and washed in TBST. Blots were imaged using the Li-Cor Odyssey Fc Imager. ImageJ (FIJI) was used for quantification of band intensity. All bands were normalized to alpha-tubulin.

References

Arnold, Eveline Sun. 2012. *ALS-Linked TDP-43 Mutations Produce Aberrant RNA Splicing*

and Adult-Onset Motor Disease Without Aggregation Or Loss of Nuclear TDP-43. University of California, San Diego.

Barmada, Sami J., Gaia Skibinski, Erica Korb, Elizabeth J. Rao, Jane Y. Wu, and Steven Finkbeiner. 2010. "Cytoplasmic Mislocalization of TDP-43 Is Toxic to Neurons and Enhanced by a Mutation Associated with Familial Amyotrophic Lateral Sclerosis." *The Journal of Neuroscience: The Official Journal of the Society for Neuroscience* 30 (2): 639–49.

Barton, Samantha K., Dario Magnani, Owen G. James, Matthew R. Livesey, Bhuvaneish T. Selvaraj, Owain T. James, Emma M. Perkins, et al. 2021. "Transactive Response DNA-Binding Protein-43 Proteinopathy in Oligodendrocytes Revealed Using an Induced Pluripotent Stem Cell Model." *Brain Communications* 3 (4): fcab255.

Baughn, Michael W., Ze 'ev Melamed, Jone López-Erauskin, Melinda S. Beccari, Karen Ling, Aamir Zuberi, Maximilliano Presa, et al. 2023. "Mechanism of STMN2 Cryptic Splice-Polyadenylation and Its Correction for TDP-43 Proteinopathies." *Science* 379 (6637): 1140–49.

Boer, Eva Maria Johanna de, Viyanti K. Orie, Timothy Williams, Mark R. Baker, Hugo M. De Oliveira, Tuomo Polvikoski, Matthew Silsby, et al. 2020. "TDP-43 Proteinopathies: A New Wave of Neurodegenerative Diseases." *Journal of Neurology, Neurosurgery, and Psychiatry* 92 (1): 86–95.

Brown, Anna-Leigh, Oscar G. Wilkins, Matthew J. Keuss, Sarah E. Hill, Matteo Zanovello, Weaverly Colleen Lee, Alexander Bampton, et al. 2022. "TDP-43 Loss and ALS-Risk SNPs Drive Mis-Splicing and Depletion of UNC13A." *Nature* 603 (7899): 131–37.

Brown, Robert H., and Ammar Al-Chalabi. 2017. "Amyotrophic Lateral Sclerosis." *The New England Journal of Medicine* 377 (2): 162–72.

Buratti, Emanuele, Laura De Conti, Cristiana Stuani, Maurizio Romano, Marco Baralle, and Francisco Baralle. 2010. "Nuclear Factor TDP-43 Can Affect Selected microRNA Levels." *The FEBS Journal* 277 (10): 2268–81.

Chu, Jen-Fei, Pritha Majumder, Biswanath Chatterjee, Shih-Ling Huang, and Che-Kun James Shen. 2019. "TDP-43 Regulates Coupled Dendritic mRNA Transport-Translation Processes in Co-Operation with FMRP and Staufen1." *Cell Reports* 29 (10): 3118–33.e6.

Dobin, Alexander, Carrie A. Davis, Felix Schlesinger, Jorg Drenkow, Chris Zaleski, Sonali Jha, Philippe Batut, Mark Chaisson, and Thomas R. Gingeras. 2013. "STAR: Ultrafast Universal RNA-Seq Aligner." *Bioinformatics* 29 (1): 15–21.

Donde, Aneesh, Mingkuan Sun, Jonathan P. Ling, Kerstin E. Braunstein, Bo Pang, Xinrui Wen, Xueying Cheng, Liam Chen, and Philip C. Wong. 2019. "Splicing Repression Is a Major Function of TDP-43 in Motor Neurons." *Acta Neuropathologica* 138 (5): 813–26.

Emde, Anna, Chen Eitan, Lee-Loung Liou, Ryan T. Libby, Natali Rivkin, Iddo Magen, Irit Reichenstein, et al. 2015. “Dysregulated miRNA Biogenesis Downstream of Cellular Stress and ALS-Causing Mutations: A New Mechanism for ALS.” *The EMBO Journal* 34 (21): 2633–51.

Farrants, Helen, Miroslaw Tarnawski, Thorsten G. Müller, Shotaro Otsuka, Julien Hiblot, Birgit Koch, Moritz Kueblbeck, Hans-Georg Kräusslich, Jan Ellenberg, and Kai Johnsson. 2020. “Chemogenetic Control of Nanobodies.” *Nature Methods* 17 (3): 279–82.

Figueroa-Romero, Claudia, Junguk Hur, J. Simon Lunn, Ximena Paez-Colasante, Diane E. Bender, Raymond Yung, Stacey A. Sakowski, and Eva L. Feldman. 2016. “Expression of microRNAs in Human Post-Mortem Amyotrophic Lateral Sclerosis Spinal Cords Provides Insight into Disease Mechanisms.” *Molecular and Cellular Neurosciences* 71 (March): 34–45.

Friedländer, Marc R., Wei Chen, Catherine Adamidi, Jonas Maaskola, Ralf Einspanier, Signe Knespel, and Nikolaus Rajewsky. 2008. “Discovering microRNAs from Deep Sequencing Data Using miRDeep.” *Nature Biotechnology* 26 (4): 407–15.

Gagliardi, Delia, Giacomo P. Comi, Nereo Bresolin, and Stefania Corti. 2019. “MicroRNAs as Regulators of Cell Death Mechanisms in Amyotrophic Lateral Sclerosis.” *Journal of Cellular and Molecular Medicine* 23 (3): 1647–56.

Giacomelli, Elisa, Björn F. Vahsen, Elizabeth L. Calder, Yinyan Xu, Jakub Scaber, Elizabeth Gray, Ruxandra Dafinca, Kevin Talbot, and Lorenz Studer. 2022. “Human Stem Cell Models of Neurodegeneration: From Basic Science of Amyotrophic Lateral Sclerosis to Clinical Translation.” *Cell Stem Cell* 29 (1): 11–35.

Gimenez, Juliette, Alida Spalloni, Sara Cappelli, Francesca Ciaiola, Valerio Orlando, Emanuele Buratti, and Patrizia Longone. 2023. “TDP-43 Epigenetic Facets and Their Neurodegenerative Implications.” *International Journal of Molecular Sciences* 24 (18). https://doi.org/10.3390/ijms241813807.

Hardiman, Orla, Ammar Al-Chalabi, Adriano Chio, Emma M. Corr, Giancarlo Logroscino, Wim Robberecht, Pamela J. Shaw, Zachary Simmons, and Leonard H. van den Berg. 2017. “Amyotrophic Lateral Sclerosis.” *Nature Reviews. Disease Primers* 3 (October): 17071.

Hawkins, Sophie, Seema C. Namboori, Ammarah Tariq, Catherine Blaker, Christine Flaxman, Nidhi S. Dey, Peter Henley, et al. 2022. “Upregulation of β-Catenin Due to Loss of miR-139 Contributes to Motor Neuron Death in Amyotrophic Lateral Sclerosis.” *Stem Cell Reports* 17 (7): 1650–65.

James, Owen G., Bhuvaneish T. Selvaraj, Dario Magnani, Karen Burr, Peter Connick, Samantha K. Barton, Navneet A. Vasistha, et al. 2022. “iPSC-Derived Myelinoids to

Study Myelin Biology of Humans." *Developmental Cell* 57 (1): 146.

Kawahara, Yukio, and Ai Mieda-Sato. 2012. "TDP-43 Promotes microRNA Biogenesis as a Component of the Drosha and Dicer Complexes." *Proceedings of the National Academy of Sciences of the United States of America* 109 (9): 3347–52.

Klim, Joseph R., Luis A. Williams, Francesco Limone, Irune Guerra San Juan, Brandi N. Davis-Dusenbery, Daniel A. Mordes, Aaron Burberry, et al. 2019. "ALS-Implicated Protein TDP-43 Sustains Levels of STMN2, a Mediator of Motor Neuron Growth and Repair." *Nature Neuroscience* 22 (2): 167–79.

Leung, Szi Kay, Aaron R. Jeffries, Isabel Castanho, Rosemary A. Bamford, Karen Moore, Emma L. Dempster, Jonathan T. Brown, et al. 2023. "Long-Read Transcript Sequencing Identifies Differential Isoform Expression in the Entorhinal Cortex in a Transgenic Model of Tau Pathology." *bioRxiv*. https://doi.org/10.1101/2023.09.20.558220.

Liao, Yang, Gordon K. Smyth, and Wei Shi. 2014. "featureCounts: An Efficient General Purpose Program for Assigning Sequence Reads to Genomic Features." *Bioinformatics* 30 (7): 923–30.

Licht-Murava, Avital, Samantha M. Meadows, Fernando Palaguachi, Soomin C. Song, Stephanie Jackvony, Yaron Bram, Constance Zhou, et al. 2023. "Astrocytic TDP-43 Dysregulation Impairs Memory by Modulating Antiviral Pathways and Interferon-Inducible Chemokines." *Science Advances* 9 (16): eade1282.

Li, Heng. 2018. "Minimap2: Pairwise Alignment for Nucleotide Sequences." *Bioinformatics* 34 (18): 3094–3100.

Ling, Jonathan P., Olga Pletnikova, Juan C. Troncoso, and Philip C. Wong. 2015. "TDP-43 Repression of Nonconserved Cryptic Exons Is Compromised in ALS-FTD." *Science* 349 (6248): 650–55.

Ling, Shuo-Chien, Magdalini Polymenidou, and Don W. Cleveland. 2013. "Converging Mechanisms in ALS and FTD: Disrupted RNA and Protein Homeostasis." *Neuron* 79 (3): 416–38.

Li, Yang I., David A. Knowles, Jack Humphrey, Alvaro N. Barbeira, Scott P. Dickinson, Hae Kyung Im, and Jonathan K. Pritchard. 2018. "Annotation-Free Quantification of RNA Splicing Using LeafCutter." *Nature Genetics* 50 (1): 151–58.

Love, Michael I., Wolfgang Huber, and Simon Anders. 2014. "Moderated Estimation of Fold Change and Dispersion for RNA-Seq Data with DESeq2." *Genome Biology* 15 (12): 550.

Ma, X. Rosa, Mercedes Prudencio, Yuka Koike, Sarat C. Vatsavayai, Garam Kim, Fred Harbinski, Adam Briner, et al. 2022. "TDP-43 Represses Cryptic Exon Inclusion in the FTD-ALS Gene UNC13A." *Nature* 603 (7899): 124–30.

McMillan, Michael, Nicolas Gomez, Caroline Hsieh, Michael Bekier, Xingli Li, Roberto

Miguez, Elizabeth M. H. Tank, and Sami J. Barmada. 2023. “RNA Methylation Influences TDP43 Binding and Disease Pathogenesis in Models of Amyotrophic Lateral Sclerosis and Frontotemporal Dementia.” *Molecular Cell* 83 (2): 219–36.e7.

Melamed, Ze ’ev, Jone López-Erauskin, Michael W. Baughn, Ouyang Zhang, Kevin Drenner, Ying Sun, Fernande Freyermuth, et al. 2019. “Premature Polyadenylation-Mediated Loss of Stathmin-2 Is a Hallmark of TDP-43-Dependent Neurodegeneration.” *Nature Neuroscience* 22 (2): 180–90.

Nagano, Seiichi, Junki Jinno, Rehab F. Abdelhamid, Yinshi Jin, Megumi Shibata, Shohei Watanabe, Sachiko Hirokawa, et al. 2020. “TDP-43 Transports Ribosomal Protein mRNA to Regulate Axonal Local Translation in Neuronal Axons.” *Acta Neuropathologica* 140 (5): 695–713.

Namboori, Seema C., Patricia Thomas, Ryan Ames, Sophie Hawkins, Lawrence O. Garrett, Craig R. G. Willis, Alessandro Rosa, Lawrence W. Stanton, and Akshay Bhinge. 2021. “Single-Cell Transcriptomics Identifies Master Regulators of Neurodegeneration in SOD1 ALS iPSC-Derived Motor Neurons.” *Stem Cell Reports* 16 (12): 3020–35.

Neumann, Manuela, Deepak M. Sampathu, Linda K. Kwong, Adam C. Truax, Matthew C. Micsenyi, Thomas T. Chou, Jennifer Bruce, et al. 2006. “Ubiquitinated TDP-43 in Frontotemporal Lobar Degeneration and Amyotrophic Lateral Sclerosis.” *Science* 314 (5796): 130–33.

Paez-Colasante, Ximena, Claudia Figueroa-Romero, Amy E. Rumora, Junguk Hur, Faye E. Mendelson, John M. Hayes, Carey Backus, et al. 2020. “Cytoplasmic TDP43 Binds microRNAs: New Disease Targets in Amyotrophic Lateral Sclerosis.” *Frontiers in Cellular Neuroscience* 14 (May): 117.

Polymenidou, Magdalini, Clotilde Lagier-Tourenne, Kasey R. Hutt, Stephanie C. Huelga, Jacqueline Moran, Tiffany Y. Liang, Shuo-Chien Ling, et al. 2011. “Long Pre-mRNA Depletion and RNA Missplicing Contribute to Neuronal Vulnerability from Loss of TDP-43.” *Nature Neuroscience* 14 (4): 459–68.

Qian, Kun, Cindy Tzu-Ling Huang, Hong Chen, Lisle W. Blackbourn 4th, Yuejun Chen, Jingyuan Cao, Lin Yao, Cornall Sauvey, Zhongwei Du, and Su-Chun Zhang. 2014. “A Simple and Efficient System for Regulating Gene Expression in Human Pluripotent Stem Cells and Derivatives.” *Stem Cells* 32 (5): 1230–38.

Reichenstein, Irit, Chen Eitan, Sandra Diaz-Garcia, Guy Haim, Iddo Magen, Aviad Siany, Mariah L. Hoye, et al. 2019. “Human Genetics and Neuropathology Suggest a Link between miR-218 and Amyotrophic Lateral Sclerosis Pathophysiology.” *Science Translational Medicine* 11 (523). https://doi.org/10.1126/scitranslmed.aav5264.

Sathyan, Kizhakke Mattada, Brian D. McKenna, Warren D. Anderson, Fabiana M. Duarte, Leighton Core, and Michael J. Guertin. 2019. “An Improved Auxin-Inducible Degron

System Preserves Native Protein Levels and Enables Rapid and Specific Protein Depletion." *Genes & Development* 33 (19-20): 1441–55.

Sidibé, Hadjara, Yousra Khalfallah, Shangxi Xiao, Nicolás B. Gómez, Hana Fakim, Elizabeth M. H. Tank, Geneviève Di Tomasso, et al. 2021. "TDP-43 Stabilizes G3BP1 mRNA: Relevance to Amyotrophic Lateral Sclerosis/frontotemporal Dementia." *Brain: A Journal of Neurology* 144 (11): 3461–76.

Smethurst, Phillip, Emmanuel Risse, Giulia E. Tyzack, Jamie S. Mitchell, Doaa M. Taha, Yun-Ru Chen, Jia Newcombe, John Collinge, Katie Sidle, and Rickie Patani. 2020. "Distinct Responses of Neurons and Astrocytes to TDP-43 Proteinopathy in Amyotrophic Lateral Sclerosis." *Brain: A Journal of Neurology* 143 (2): 430–40.

Stirling, David R., Madison J. Swain-Bowden, Alice M. Lucas, Anne E. Carpenter, Beth A. Cimini, and Allen Goodman. 2021. "CellProfiler 4: Improvements in Speed, Utility and Usability." *BMC Bioinformatics* 22 (1): 433.

Tam, Oliver H., Nikolay V. Rozhkov, Regina Shaw, Duyang Kim, Isabel Hubbard, Samantha Fennessey, Nadia Propp, et al. 2019. "Postmortem Cortex Samples Identify Distinct Molecular Subtypes of ALS: Retrotransposon Activation, Oxidative Stress, and Activated Glia." *Cell Reports* 29 (5): 1164–77.e5.

Tang, Alison D., Cameron M. Soulette, Marijke J. van Baren, Kevyn Hart, Eva Hrabeta-Robinson, Catherine J. Wu, and Angela N. Brooks. 2020. "Full-Length Transcript Characterization of SF3B1 Mutation in Chronic Lymphocytic Leukemia Reveals Downregulation of Retained Introns." *Nature Communications* 11 (1): 1438.

Walker, Adam K., Krista J. Spiller, Guanghui Ge, Allen Zheng, Yan Xu, Melissa Zhou, Kalyan Tripathy, Linda K. Kwong, John Q. Trojanowski, and Virginia M-Y Lee. 2015. "Functional Recovery in New Mouse Models of ALS/FTLD after Clearance of Pathological Cytoplasmic TDP-43." *Acta Neuropathologica* 130 (5): 643–60.

Weskamp, Kaitlin, Elizabeth M. Tank, Roberto Miguez, Jonathon P. McBride, Nicolás B. Gómez, Matthew White, Ziqiang Lin, et al. 2020. "Shortened TDP43 Isoforms Upregulated by Neuronal Hyperactivity Drive TDP43 Pathology in ALS." *The Journal of Clinical Investigation* 130 (3): 1139–55.

Zhang, Zhijun, Sandra Almeida, Yubing Lu, Agnes L. Nishimura, Lingtao Peng, Danqiong Sun, Bei Wu, et al. 2013. "Downregulation of microRNA-9 in iPSC-Derived Neurons of FTD/ALS Patients with TDP-43 Mutations." *PloS One* 8 (10): e76055.

Ziff, Oliver J., Jasmine Harley, Yiran Wang, Jacob Neeves, Giulia Tyzack, Fairouz Ibrahim, Mark Skehel, Anob M. Chakrabarti, Gavin Kelly, and Rickie Patani. 2023. "Nucleocytoplasmic mRNA Redistribution Accompanies RNA Binding Protein Mislocalization in ALS Motor Neurons and Is Restored by VCP ATPase Inhibition." *Neuron* 111 (19): 3011–27.e7.

Zuo, Xinxin, Jie Zhou, Yinming Li, Kai Wu, Zonggui Chen, Zhiwei Luo, Xiaorong Zhang, et al. 2021. “TDP-43 Aggregation Induced by Oxidative Stress Causes Global Mitochondrial Imbalance in ALS.” *Nature Structural & Molecular Biology* 28 (2): 132–42.

Figure 1

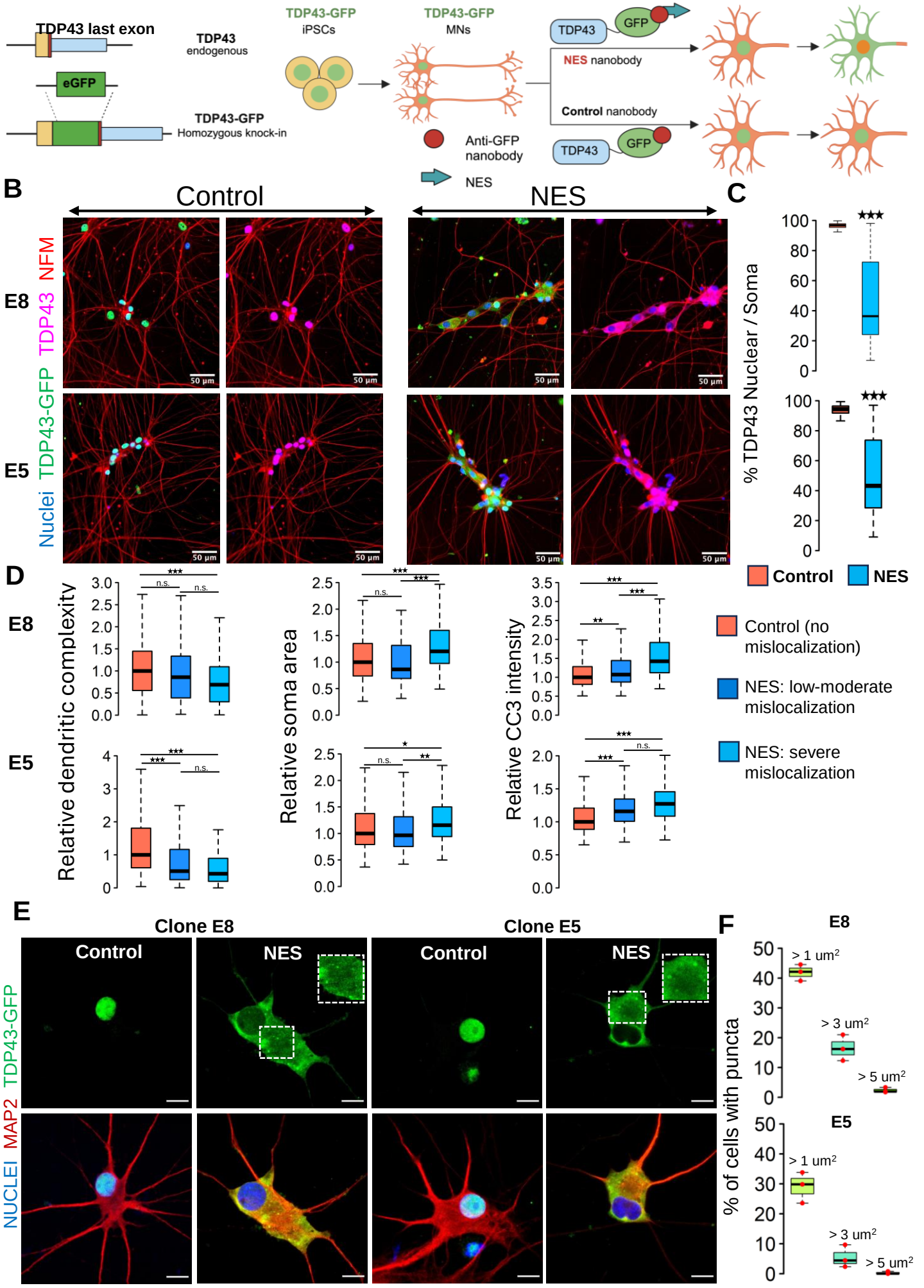
A
TDP43 last exon
TDP43
endogenous
eGFP
TDP43-GFP
Homozygous knock-in
TDP43-GFP
iPSCs
TDP43-GFP
MNs
Anti-GFP
nanobody
NES
TDP43
GFP
NES nanobody
Control nanobody
B
Control
NES
E8
E5
NFM
TDP43
TDP43-GFP
Nuclei
50 µm
C
% TDP43 Nuclear / Soma
Control
NES
D
Relative dendritic complexity
Relative soma area
Relative CC3 intensity
n.s.
Control (no mislocalization)
NES: low-moderate mislocalization
NES: severe mislocalization
E
Clone E8
Clone E5
Control
NES
TDP43-GFP
MAP2
NUCLEI
F
E8
E5
% of cells with puncta
> 1 um²
> 3 um²
> 5 um²

Figure 1. A Human iPSC-based model of TDP43 proteinopathy in MNs

(A) Schematic depicting genome editing of healthy iPSCs to knock-in GFP into the C-terminus of endogenous *TARDBP*, encoding TDP43. Yellow rectangle indicates the TDP43 last exon. Red vertical line indicates the STOP codon. Blue rectangle indicates the TDP43 3'UTR. The resulting TDP43-GFP iPSCs are differentiated into motor neurons (MNs) and transduced with AAVs encoding anti-GFP nanobodies. The "NES" nanobody includes a sequence for a strong nuclear export signal, which transports nuclear TDP43-GFP into the cytoplasm. The control nanobody (lacking NES) has no effect on TDP43-GFP localization.

(B) Representative images depicting TDP43 localization in two homozygous TDP43-GFP lines (E8, E5). MNs were transduced at day 20 of the differentiation process and fixed at day 40 for the immunostaining. TDP43 is expressed in the nucleus in the presence of the control nanobody and relocates to the cytoplasm in the presence of the NES nanobody. TDP43-GFP indicates signal from the anti-GFP antibody while TDP43 indicates signal from the anti-TDP43 antibody. Neurons were also stained with neurofilament-M (red) and Hoechst 33342 (blue nuclear stain). Scale bar = 50 µm.

(C) Quantification of the % of nuclear TDP43 intensity over total TDP43 intensity in the nucleus + soma in individual neurons transduced with control or NES nanobodies.

(D) Quantification of morphological defects and cleaved caspase 3 (CC3) levels in NES nanobody treated MNs versus control. Mislocalized TDP43 (NES) causes a reduction in dendritic complexity (D), soma swelling and elevation of CC3 levels, compared to neurons expressing nuclear TDP43 (control). Low-to-moderate mislocalization indicates neurons with > 40% nuclear TDP43. Severe mislocalization indicates neurons with < 40% nuclear TDP43. Measurements were normalized to data from the control nanobody condition.

Panels C, and D display data for the two homozygous TDP43-GFP lines (E8 and E5), transduced with nanobodies at day 20 and fixed for staining at day 40. N = 3 independent differentiations per clone. At least 100 neurons were included per condition.

(E) Representative images showing cytoplasmic TDP43 puncta at day 40 in homozygous TDP43-GFP MNs transduced with the NES nanobody at day 18. Scale bar = 15 µm. Images were captured with the Zeiss LSM880 Airyscan.

(F) Quantification of the percentage of NES expressing neurons displaying TDP43 puncta. The largest punctum per neuron was used for the analysis. Upper panel shows data for E8 neurons while lower panel displays data for E5 neurons. N = 3 independent differentiations per clone. At least 100 neurons were included per clone for the analysis.

* indicates $p < 0.01$, ** indicates $p < 0.001$, *** indicates $p < 0.0001$.

Figure 2

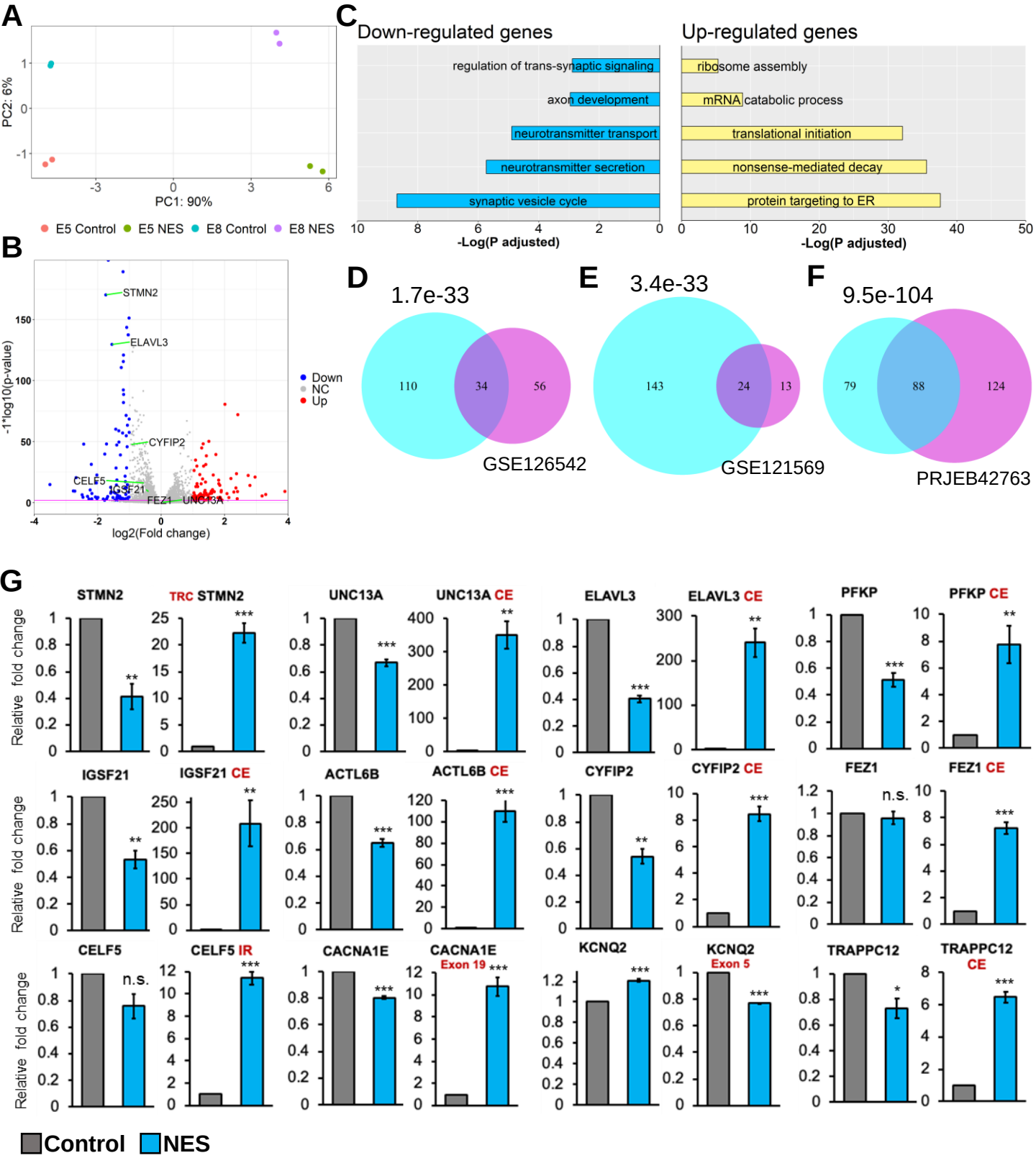
A
PC2: 6%
PC1: 90%
E5 Control
E5 NES
E8 Control
E8 NES
B
STMN2
ELAVL3
CYFIP2
CELF5
IGSF21
FEZ1
UNC13A
Down
NC
Up
-1*log10(p-value)
log2(Fold change)
C
Down-regulated genes
regulation of trans-synaptic signaling
axon development
neurotransmitter transport
neurotransmitter secretion
synaptic vesicle cycle
-Log(P adjusted)
Up-regulated genes
ribosome assembly
mRNA catabolic process
translational initiation
nonsense-mediated decay
protein targeting to ER
-Log(P adjusted)
D
1.7e-33
110
34
56
GSE126542
E
3.4e-33
143
24
13
GSE121569
F
9.5e-104
79
88
124
PRJEB42763
G
STMN2
TRC STMN2
UNC13A
UNC13A CE
ELAVL3
ELAVL3 CE
PFKP
PFKP CE
IGSF21
IGSF21 CE
ACTL6B
ACTL6B CE
CYFIP2
CYFIP2 CE
FEZ1
FEZ1 CE
CELF5
CELF5 IR
CACNA1E
CACNA1E Exon 19
KCNQ2
KCNQ2 Exon 5
TRAPPC12
TRAPPC12 CE
Relative fold change
n.s.
Control
NES

Figure 2. Transcriptional consequences of TDP43 mislocalization

(A) Principal component analysis of gene counts for E8 and E5 iPSC-MNs.

(B) Volcano plot displaying genes differentially expressed due to TDP43 mislocalization. Red: upregulated genes, Blue: downregulated genes, NC: No Change. Horizontal line denotes a p-value threshold of 0.01.

(C) Gene ontology enrichment analysis on the differentially expressed genes in the TDP43 model. The top five enriched pathways in upregulated and downregulated genes have been displayed.

(D E, F) Venn diagram displaying the overlap between mis-spliced genes identified due to TDP43 mislocalization in the TDP43-GFP iPSC MNs (cyan circles) with publicly available transcriptomic datasets; D: cortical neuronal nuclei displaying TDP43 depletion obtained from ALS/FTD patient tissue (GSE126542), E: TDP43 knockdown using siRNAs in healthy iPSC-MNs (GSE121569), F: TDP43 knockdown using CRISPRi in healthy iPSC-iNs (PRJEB42763). P-values were estimated using a hypergeometric distribution. Only genes with detectable expression in both datasets were used for splicing analysis.

(G) RT-qPCR validating alternative splicing changes resulting from TDP43-GFP mislocalization in iPSC-MNs. MN samples were lysed at day 30, 12 days post-transduction with AAVs. Replicates were three independent differentiations of homozygous TDP43-GFP knock-in lines, (two of E5, one of E8). CE = cryptic exon, TRC = truncated, IR = intron retention. *CACNA1E* and *KCNQ2* displayed alternate exon usage. The exons that were included in the NES samples have been indicated.

** indicates $p < 0.01$. *** indicates $p < 0.001$.

Figure 3

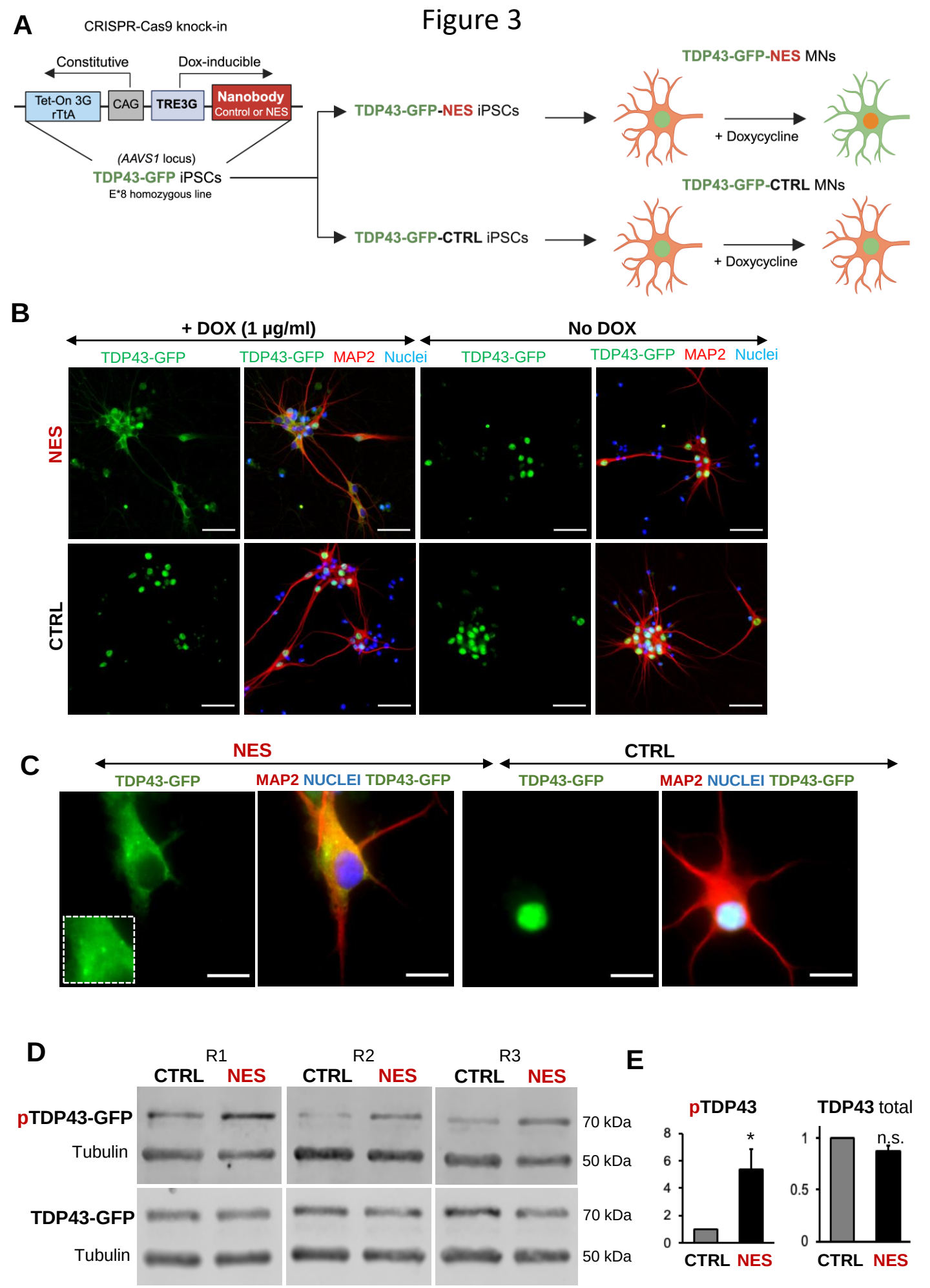
A
CRISPR-Cas9 knock-in
Constitutive
Dox-inducible
Tet-On 3G rTtA
CAG
TRE3G
Nanobody Control or NES
(AAVS1 locus)
TDP43-GFP iPSCs
E*8 homozygous line
TDP43-GFP-NES iPSCs
TDP43-GFP-CTRL iPSCs
TDP43-GFP-NES MNs
+ Doxycycline
TDP43-GFP-CTRL MNs
+ Doxycycline
B
+ DOX (1 µg/ml)
No DOX
TDP43-GFP
TDP43-GFP MAP2 Nuclei
TDP43-GFP
TDP43-GFP MAP2 Nuclei
NES
CTRL
C
NES
CTRL
TDP43-GFP
MAP2 NUCLEI TDP43-GFP
TDP43-GFP
MAP2 NUCLEI TDP43-GFP
D
R1
R2
R3
CTRL NES
CTRL NES
CTRL NES
pTDP43-GFP
Tubulin
TDP43-GFP
Tubulin
70 kDa
50 kDa
70 kDa
50 kDa
E
pTDP43
TDP43 total
8
6
4
2
0
*
1
0.5
0
n.s.
CTRL NES
CTRL NES

Figure 3. An inducible model of TDP43 mislocalization

(A) Schematic depicting the knock-in of the nanobody (control or NES) into the human *AAVS1* safe harbour locus of our E8 homozygous TDP43-GFP cell line. Nanobody expression was under the control of a doxycycline (Dox)-inducible promoter. Addition of Dox is expected to induce TDP43 mislocalization in the TDP43-GFP-NES MNs but not in the TDP43-GFP-Control (TDP43-GFP-CTRL) MNs.

(B) Immunofluorescent staining showing TDP43 localization in our TDP43-GFP-CTRL or TDP43-GFP-NES line in response to Dox. Mislocalization only occurs in the TDP43-GFP-NES line with Dox treatment, while all other conditions maintain nuclear TDP43. MNs were fixed and stained at day 35, 15 days post-Dox addition. Scale bar = 50 µm.

(C) TDP43 localization in the TDP43-GFP-NES or –CTRL cell lines at day 40, 20 days post-Dox addition. The box highlights cytoplasmic TDP43 puncta in the NES line. Scale bar = 20 µm.

(D) Western blots of total and phosphorylated TDP43 in TDP43-GFP-NES or –CTRL cell lines at day 40, 20 days post-Dox addition. Alpha-tubulin was used as a loading control.

(E) Quantification of total and phosphorylated TDP43-GFP from figure D. Total TDP43-GFP remains stable, while there is a significant increase in phosphorylated TDP43-GFP in the NES lines. Each sample was normalized to alpha-tubulin, pTDP43 samples were also normalized to total TDP43 levels. Replicates are three independent differentiations of TDP43-GFP-NES or –CTRL.

pTDP43-GFP = phosphorylated TDP43-GFP. * indicates $p < 0.05$. Error bars indicate SEM.

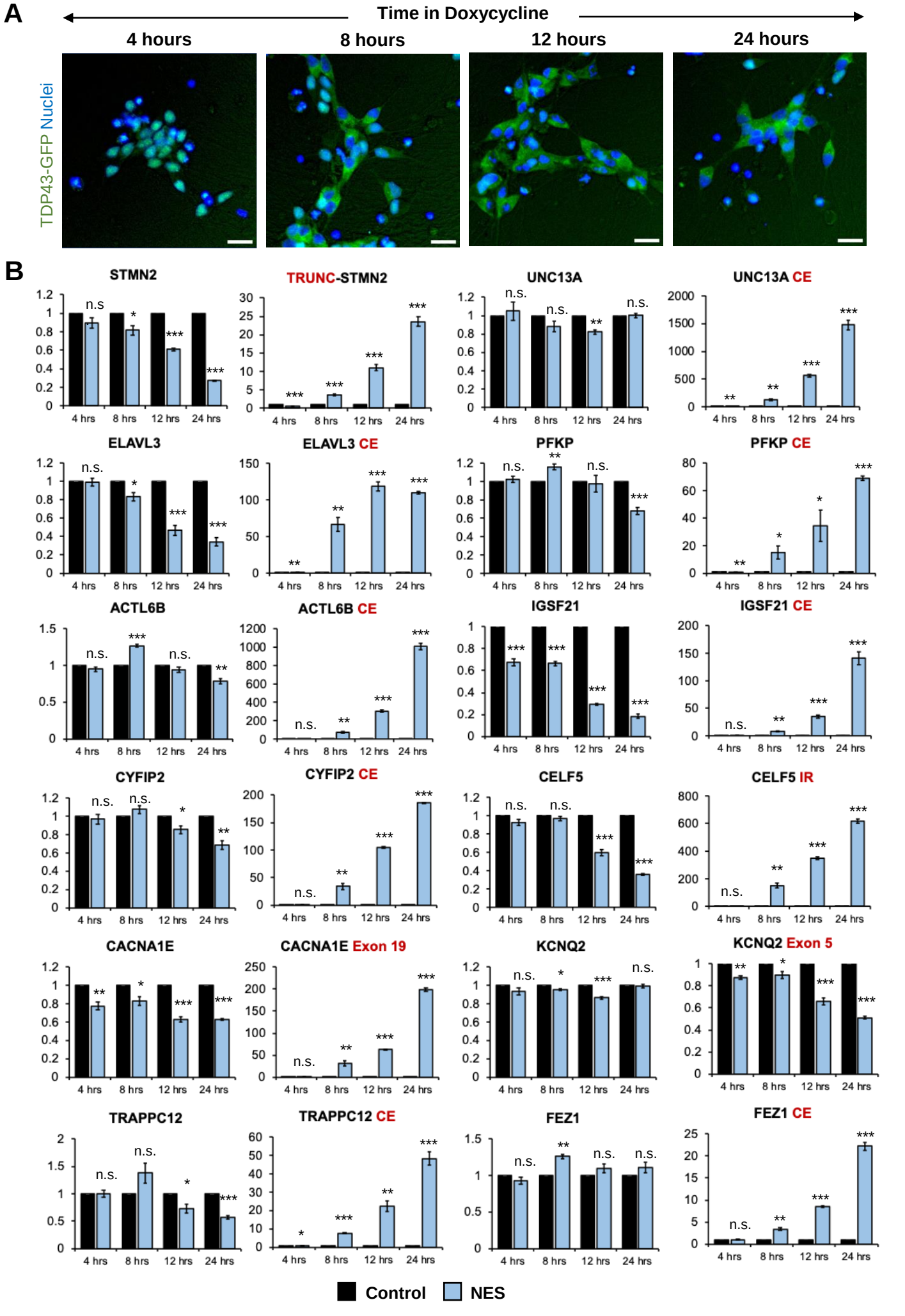
A
Time in Doxycycline
4 hours
8 hours
12 hours
24 hours
TDP43-GFP Nuclei
B
STMN2
TRUNC-STMN2
UNC13A
UNC13A CE
ELAVL3
ELAVL3 CE
PFKP
PFKP CE
ACTL6B
ACTL6B CE
IGSF21
IGSF21 CE
CYFIP2
CYFIP2 CE
CELF5
CELF5 IR
CACNA1E
CACNA1E Exon 19
KCNQ2
KCNQ2 Exon 5
TRAPPC12
TRAPPC12 CE
FEZ1
FEZ1 CE
4 hrs
8 hrs
12 hrs
24 hrs
n.s
Control
NES

Figure 4. Splicing defects are one of the earliest changes downstream of TDP43 mislocalization

(A) Immunocytochemical staining of TDP43-GFP-NES MNs at 4, 8, 12, and 24 hours following 1 ug/ml doxycycline addition. TDP43 mislocalisation is observed within 8 hours. Dox was added to MN day 20. Scale bar = 25 um.

(B) RT-qPCR of alternative splicing changes at 4, 8, 12, and 24 hours following 1 ug/ml doxycycline addition. Significant cryptic transcript expression in all genes is detected at 8 hours.
Error bars show SEM. N = 3 independent differentiations of the TDP43-GFP-CTRL/-NES lines.
CE = cryptic exon, TRC = truncated, IR = intron retention. *CACNA1E* and *KCNQ2* displayed alternate exon usage. The exons that were included in the NES samples have been indicated.

* indicates $p < 0.05$, ** indicates $p < 0.01$. *** indicates $p < 0.001$.

Figure 5

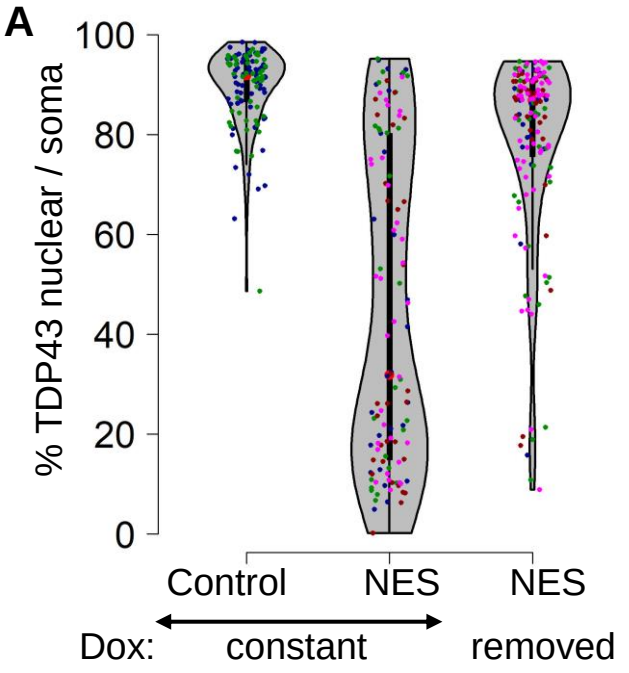
A
% TDP43 nuclear / soma
100
80
60
40
20
0
Control
NES
NES
Dox:
constant
removed

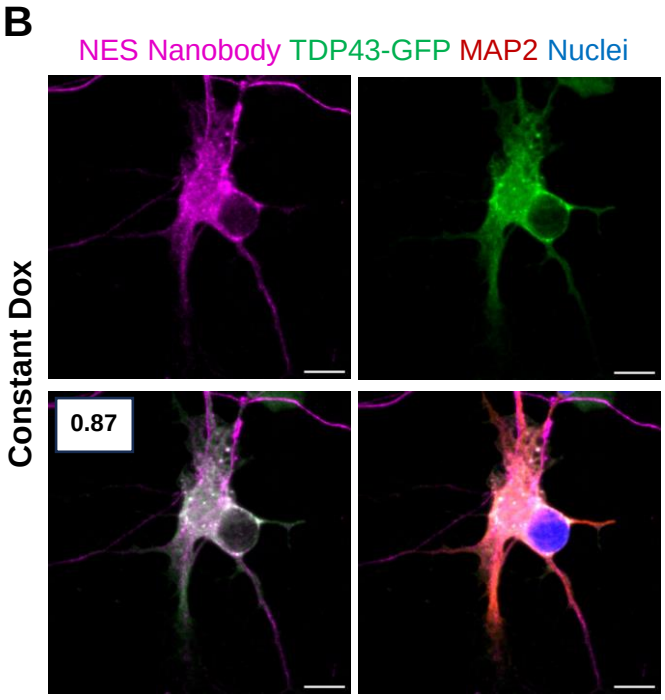
B
NES Nanobody TDP43-GFP MAP2 Nuclei
Constant Dox
0.87

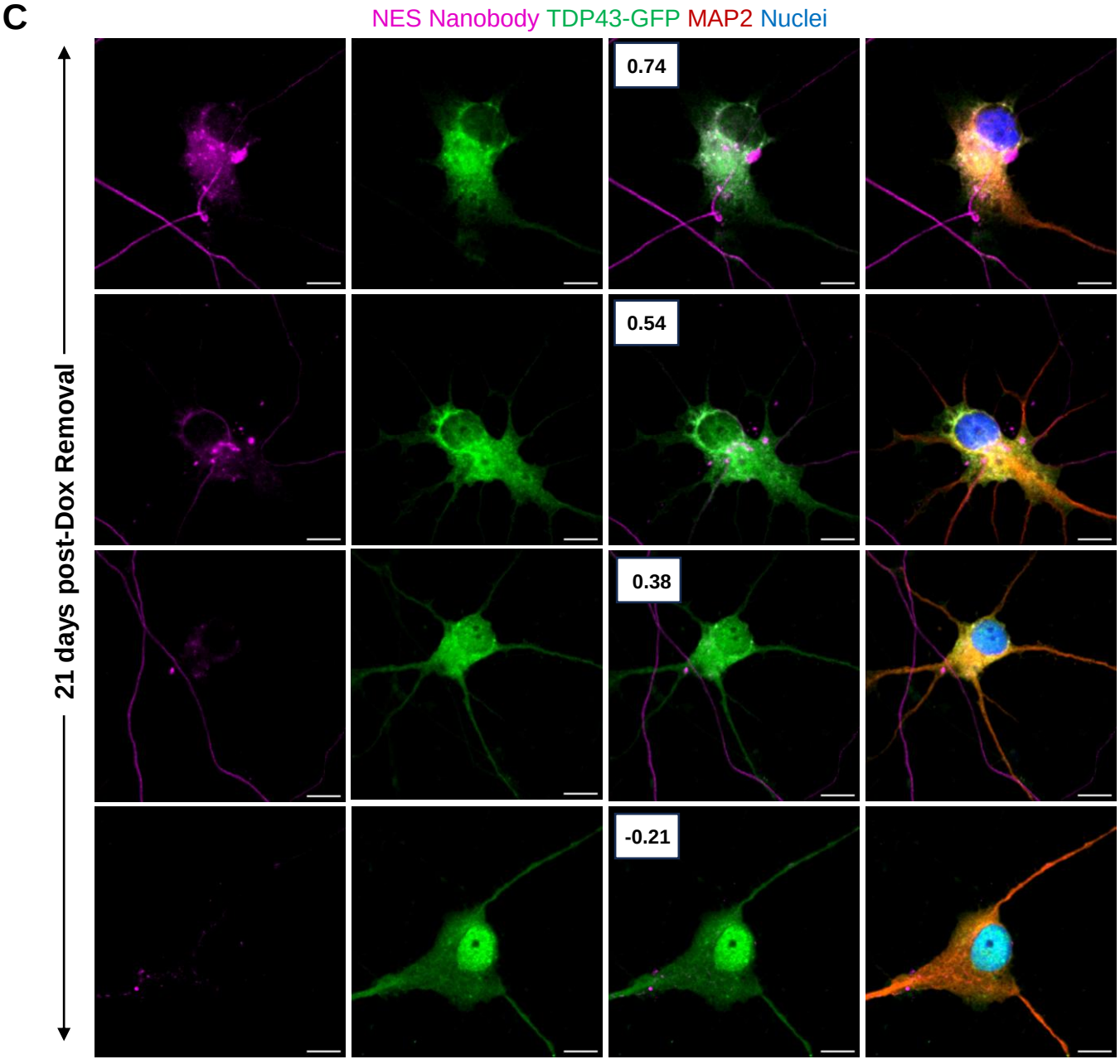
C
NES Nanobody TDP43-GFP MAP2 Nuclei
21 days post-Dox Removal
0.74
0.54
0.38
-0.21

Figure 5. Persistent mislocalization of TDP43 in neurons post-Dox withdrawal.

(A) TDP43 localization in the E8 TDP43-GFP MNs expressing dox-inducible V5-tagged nanobodies. Control: control-V5 nanobody. NES: NES-V5 nanobody. Constant: neurons were treated with dox continuously. Removed: Dox was withdrawn five days after addition.

N = 2 for the constant + control condition. N=4 for the NES conditions. Each replicate is indicated by a coloured dot. Scale bar = 20 µm.

(B, C) Representative images of the TDP43-GFP MNs expressing NES-V5 nanobody under constant dox treatment (B) and 21 days post-dox withdrawal (C).
Boxes indicate Pearson correlation coefficient between the TDP43-GFP and V5-nanobody signals across individual pixels within the soma. A higher coefficient indicates higher co-localization. Scale bar = 10 um**.** Images were captured with the Zeiss LSM880 Airyscan.

Supplementary Figure 1

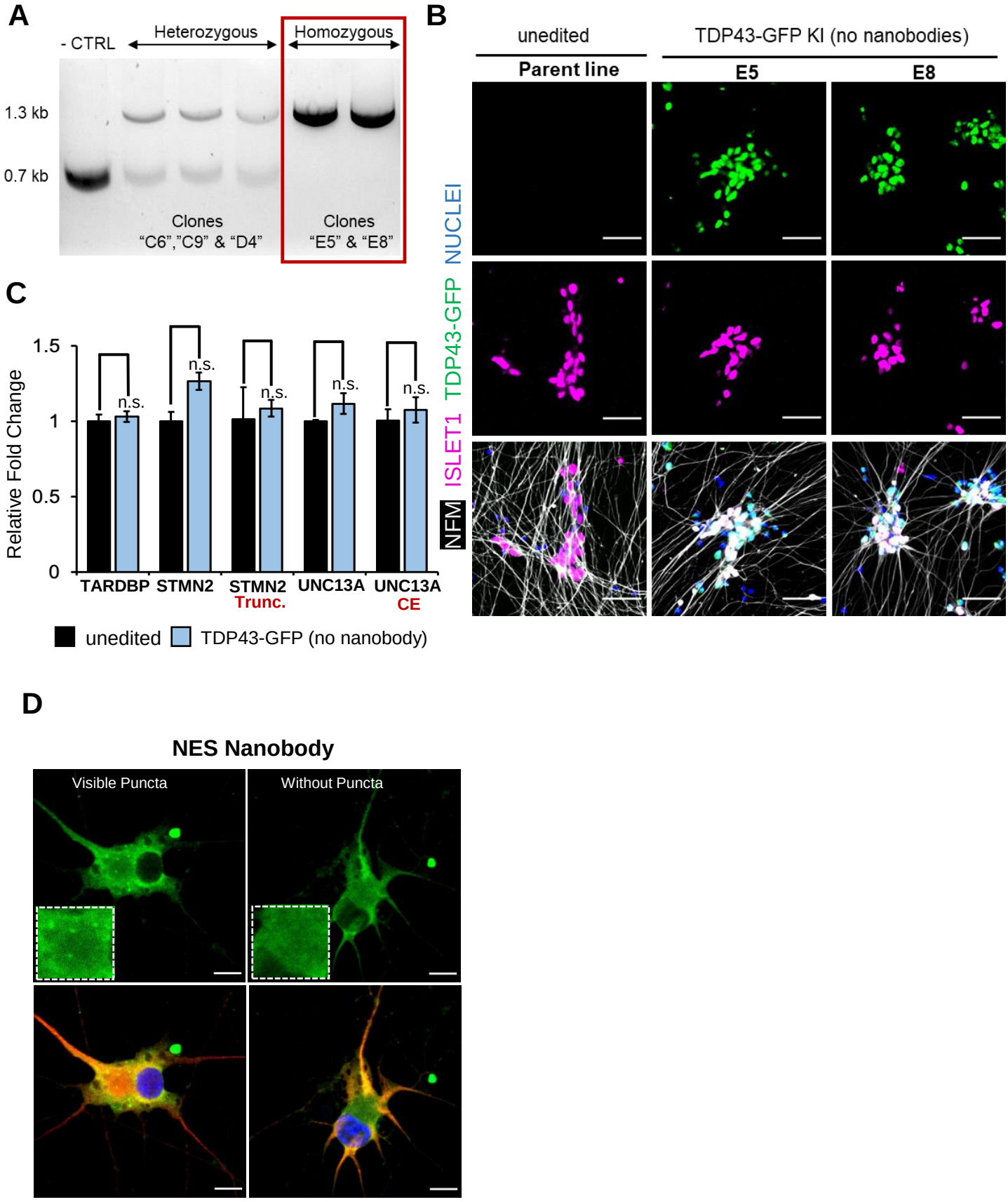

Supplementary Figure 1. Related to Figure 1

(A) Confirmation of three heterozygous and two homozygous TDP43-GFP knock-in clones using PCR-gel electrophoresis. The unedited parent healthy iPSCs served as a control. Homozygous “E5” and “E8” clones were selected.

(B) Representative images of the unedited parent line and untransduced TDP43-GFP homozygous clones E8 and E5. Neurons were stained for MN markers neurofilament-M (NFM) and ISLET1 (ISL1) at day 20. Nuclei were stained with Hoechst 33342 Scale bar = 50 µm.

(C) RT-qPCR of unedited (parent) iPSC-MNs and untransduced homozygous TDP43-GFP knock-in MNs at day 30, suggesting no adverse effects of GFP knock-in on TDP43 expression or alternative splicing. N = 3 independent differentiations for each of the unedited and TDP43-GFP (two of E5, one of E8) lines. P-values were calculated using a one-tailed Student’s T-test. Error bars show SEM. None of the differences were significant. n.s. = not significant.

(D) Representative images of the E5 homozygous TDP43-GFP line showing a cell with and without cytoplasmic puncta. Cells were fixed and stained at D40, 22 days post-transduction. Scale bar = 15 µm.

Supplementary Figure 2

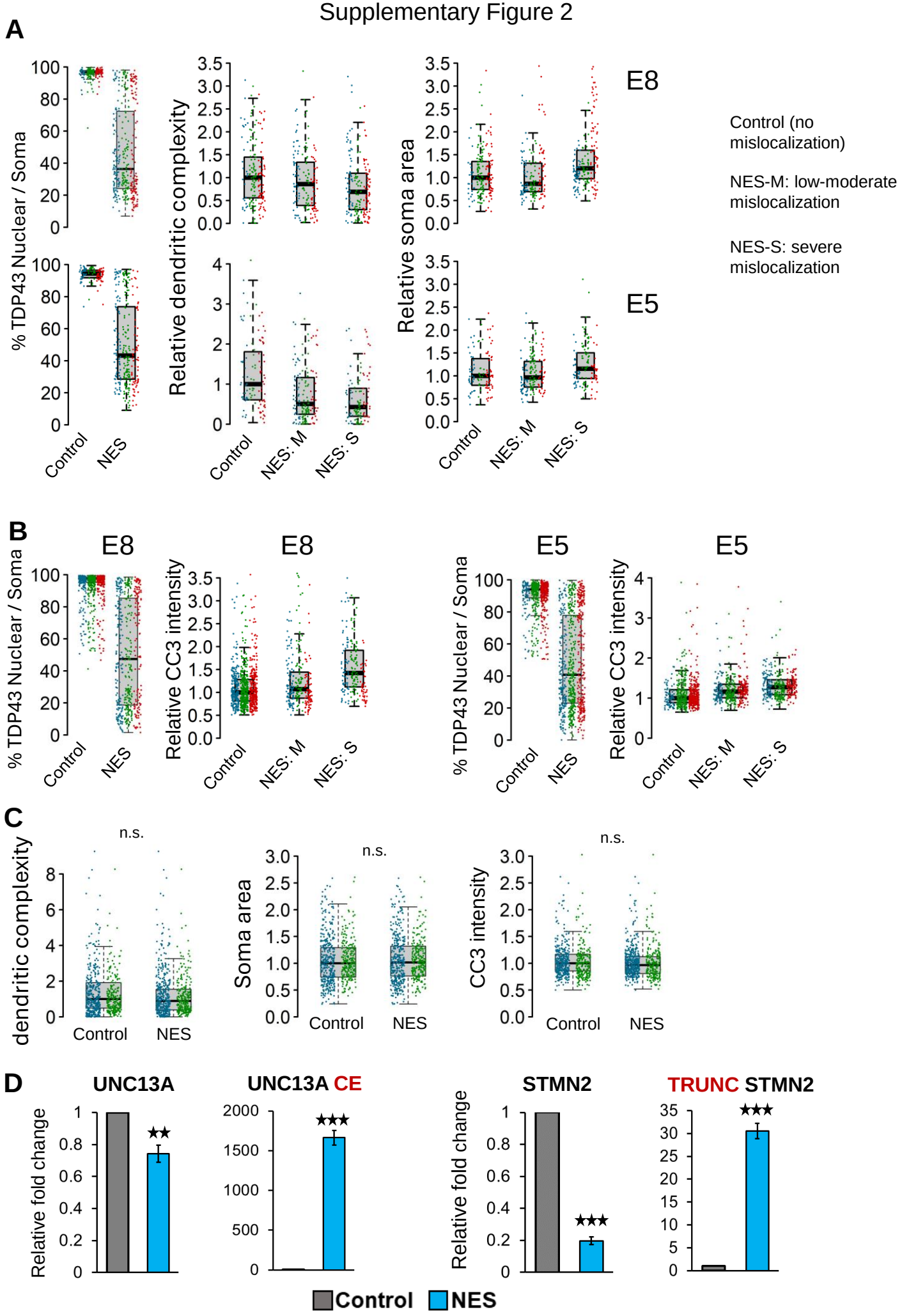

Supplementary Figure 2. Related to Figure 1

(A) Related to main figures 1C and 1D. Quantification of morphological defects in NES nanobody treated MNs versus control. Mislocalized TDP43 (NES) causes a reduction in dendritic complexity (D) and soma swelling, compared to neurons expressing nuclear TDP43 (control).

(B) Related to main figure 1D. Quantification of caspase 3 (CC3) levels in NES nanobody treated MNs versus control. Mislocalized TDP43 (NES) causes elevation of CC3 levels, compared to neurons expressing nuclear TDP43 (control).

For A and B, each replicate is indicated by a different colour. Control: control nanobody, NES: NES nanobody, NES-M: Low to moderate levels of mislocalization, defined as neurons with > 60% nuclear TDP43. NES-S: Severe mislocalization defined as neurons with < 60% nuclear TDP43.

(C) Morphological analysis in unedited (parent) iPSC MNs treated with control or NES nanobodies. No significant effect is observed on dendrite morphology, soma swelling or apoptosis (CC3 intensity) at a p-value threshold of 0.01. N = 2 independent differentiations. At least 150 neurons were analysed per condition. CC3 = cleaved caspase-3. Each replicate is indicated by a different colour.

(D) RT-qPCR showing abnormal splicing of *UNC13A* and *STMN2* in day 40 homozygous TDP43-GFP MNs, 20 days post-transduction with NES or control nanobodies. N = 6 replicates of NES and CTRL each (three of E5, three of E8). Error bars show SEM. CE = cryptic exon, TRUNC = truncated.

n.s. = not significant, ** indicates $p < 0.01$,*** indicates $p < 0.001$.

Supplementary Figure 3

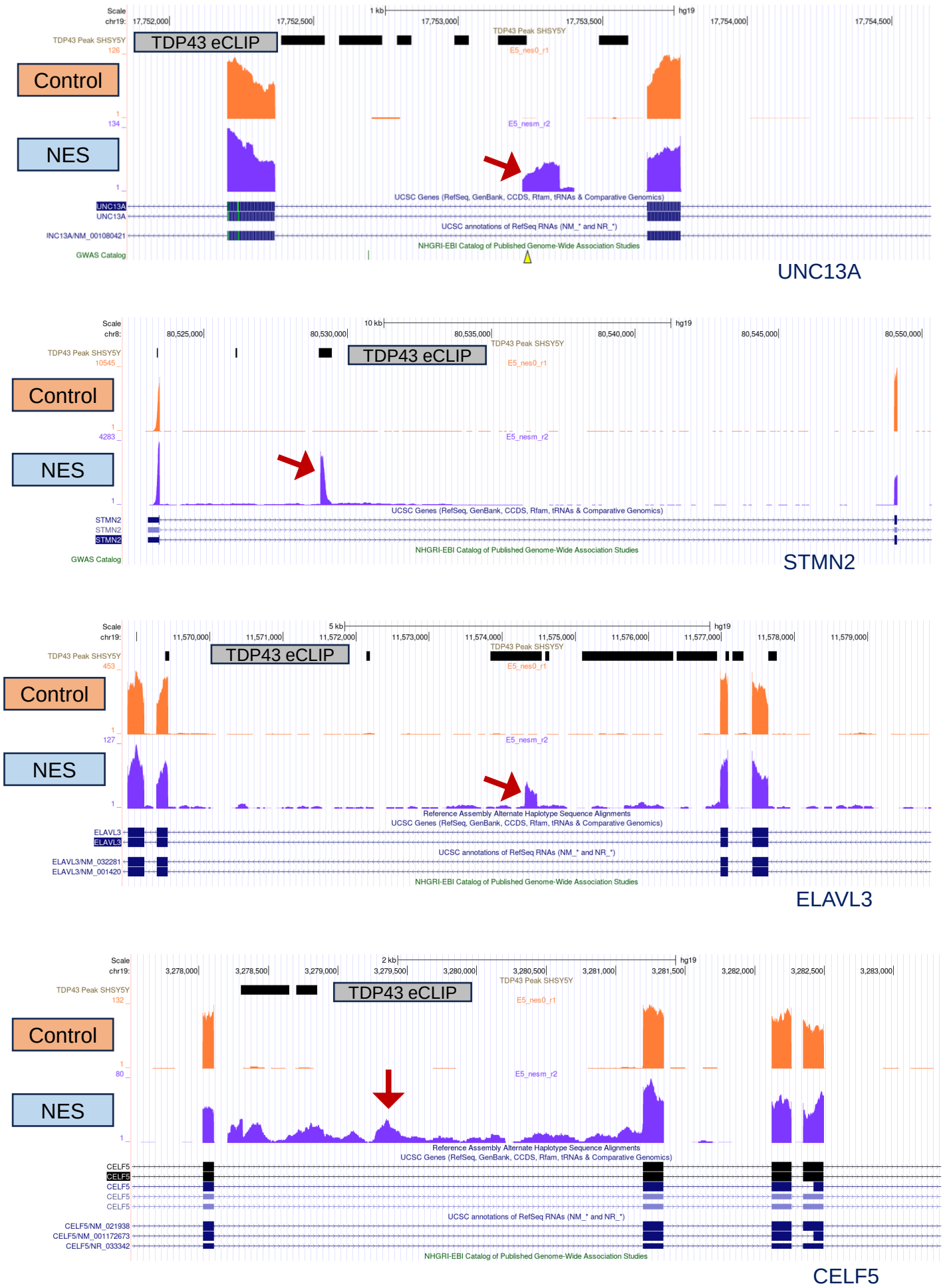

Supplementary Figure 3 (Related to Figure 2)

UCSC Genome browser screen shots depicting cryptic exon inclusion (*UNC13A, STMN2, ELAVL3*) and intron retention (*CELF5*) resulting from TDP43 mislocalization. In all cases, there is at least one TDP43 binding site, identified by SH-SY5Y eCLIP data (GSE122648) shown as a horizontal black bar. Screenshots are from the homozygous E5 TDP43-GFP clone, at MN day 40, 20 days post-transduction with AAVs. Red arrows indicate the alternative splice event.

.

Supplementary Figure 4

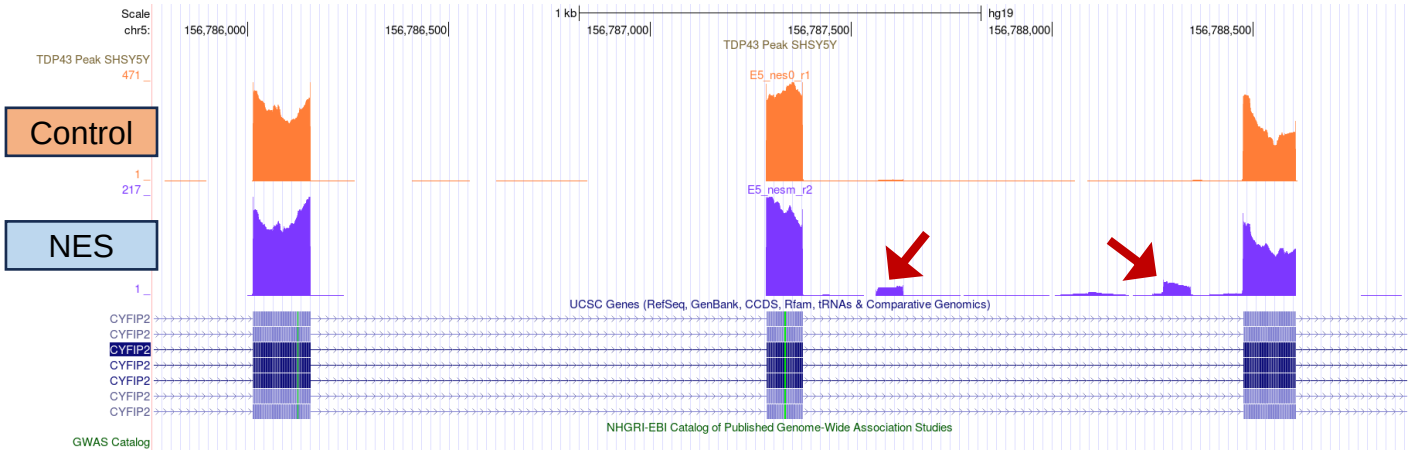

CYFIP2

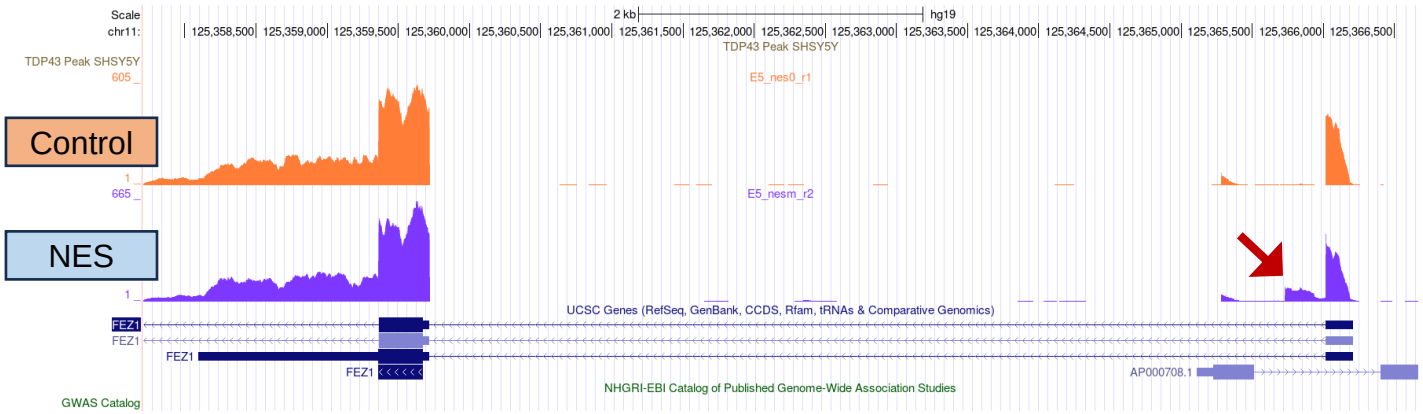

FEZ1

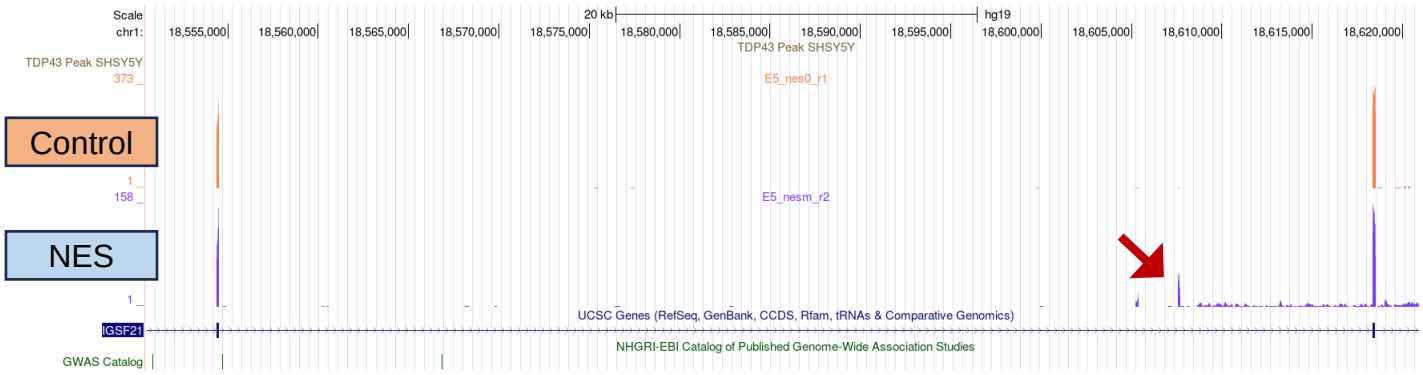

IGSF21

Supplementary Figure 4. (Related to Figure 2)

UCSC Genome browser shots depicting cryptic exon inclusion in *CYFIP2, FEZ1*, and *IGSF21* resulting from TDP43 mislocalization. There are no TDP43 binding sites identified by SH-SY5Y eCLIP data (GSE122648). Screenshots are from the homozygous E5 TDP43-GFP clone, at MN day 40, 20 days post-transduction with AAVs. Red arrows indicate the alternative splice event.

.

Supplementary Figure 5

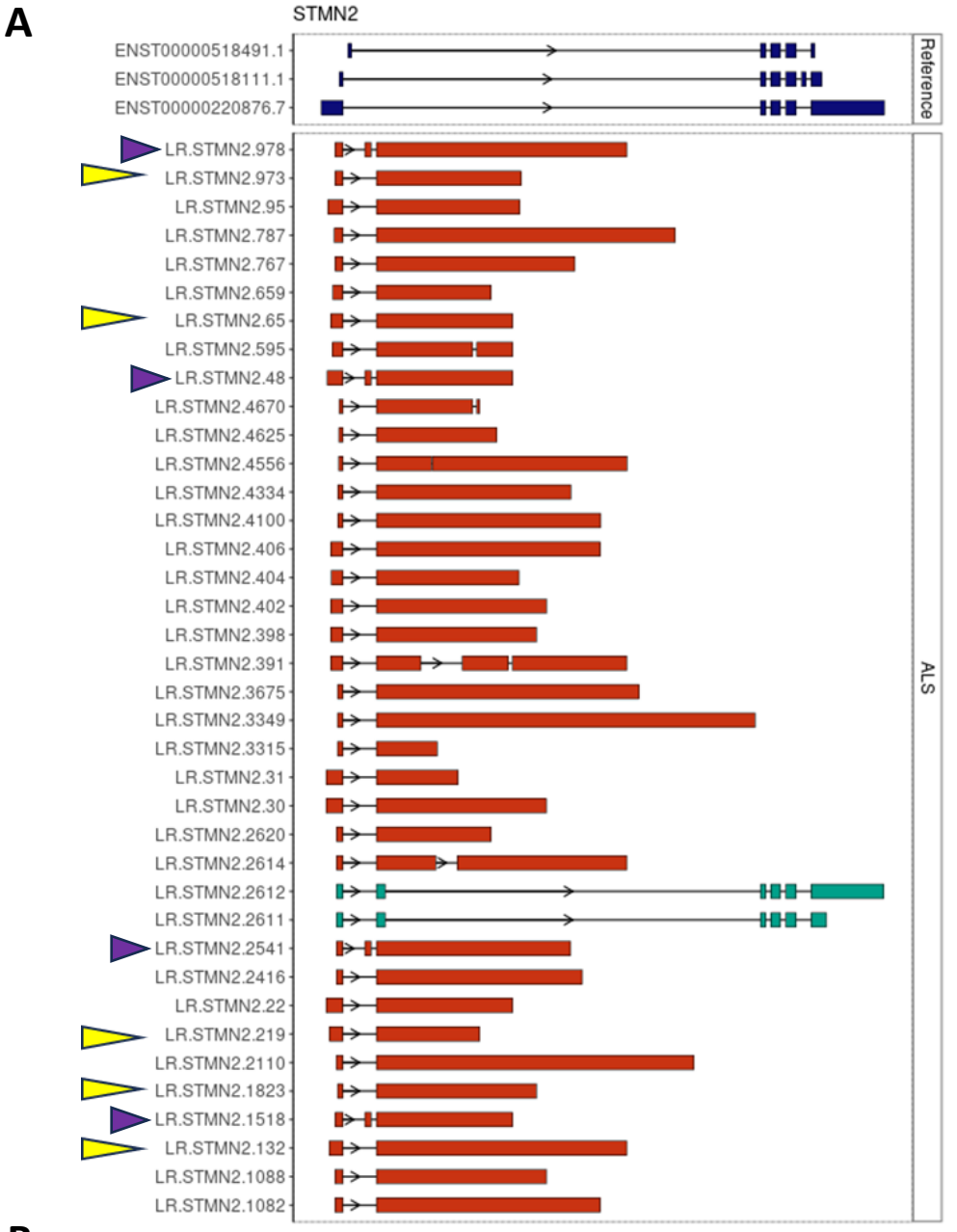

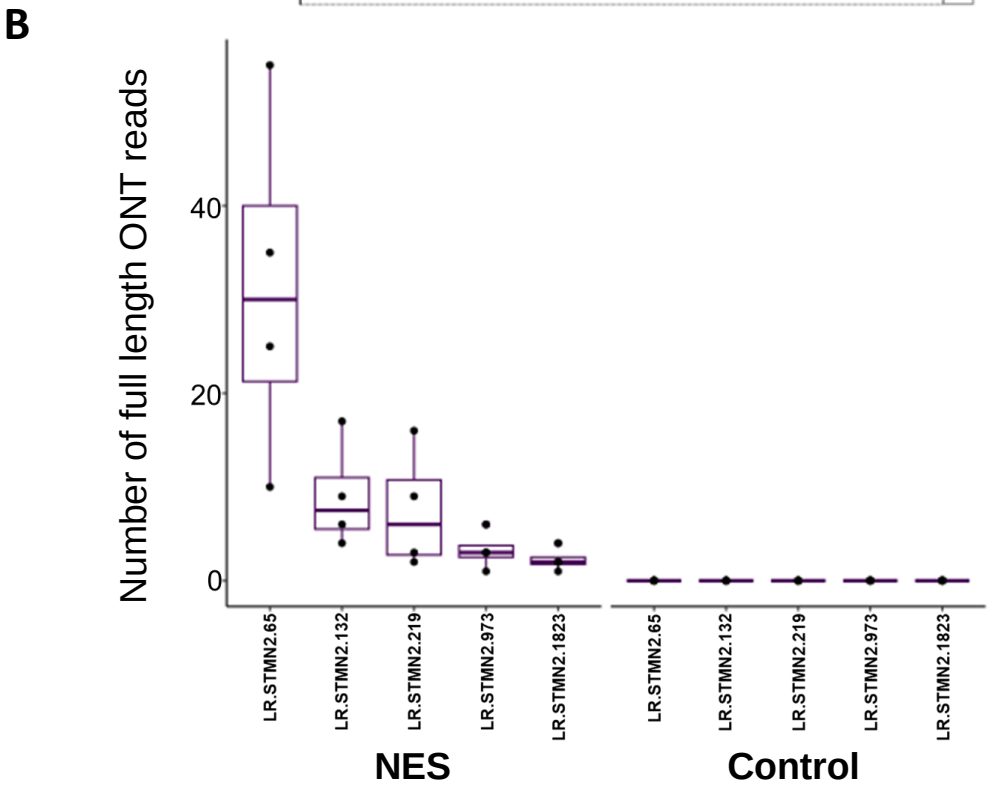

Supplementary Figure 5. (Related to Figure 2)

(A) *STMN2* transcripts containing the CE in the TDP43-GFP MNs expressing the NES nanobody (isoforms containing the variable length CE are shown in red, reference isoforms are show in dark blue at the top). Each isoform was assigned a unique number. Top five most abundant isoforms are marked by yellow arrows. Isoforms containing the extra 114 bp exon upstream of the CE are marked by purple arrows. **(B)** Quantification of the top five most abundant *STMN2* isoforms in TDP43-GFP MNs expressing control or NES nanobody**.** Each dot represent data from an independent replicate. N=4.

Supplementary Figure 6

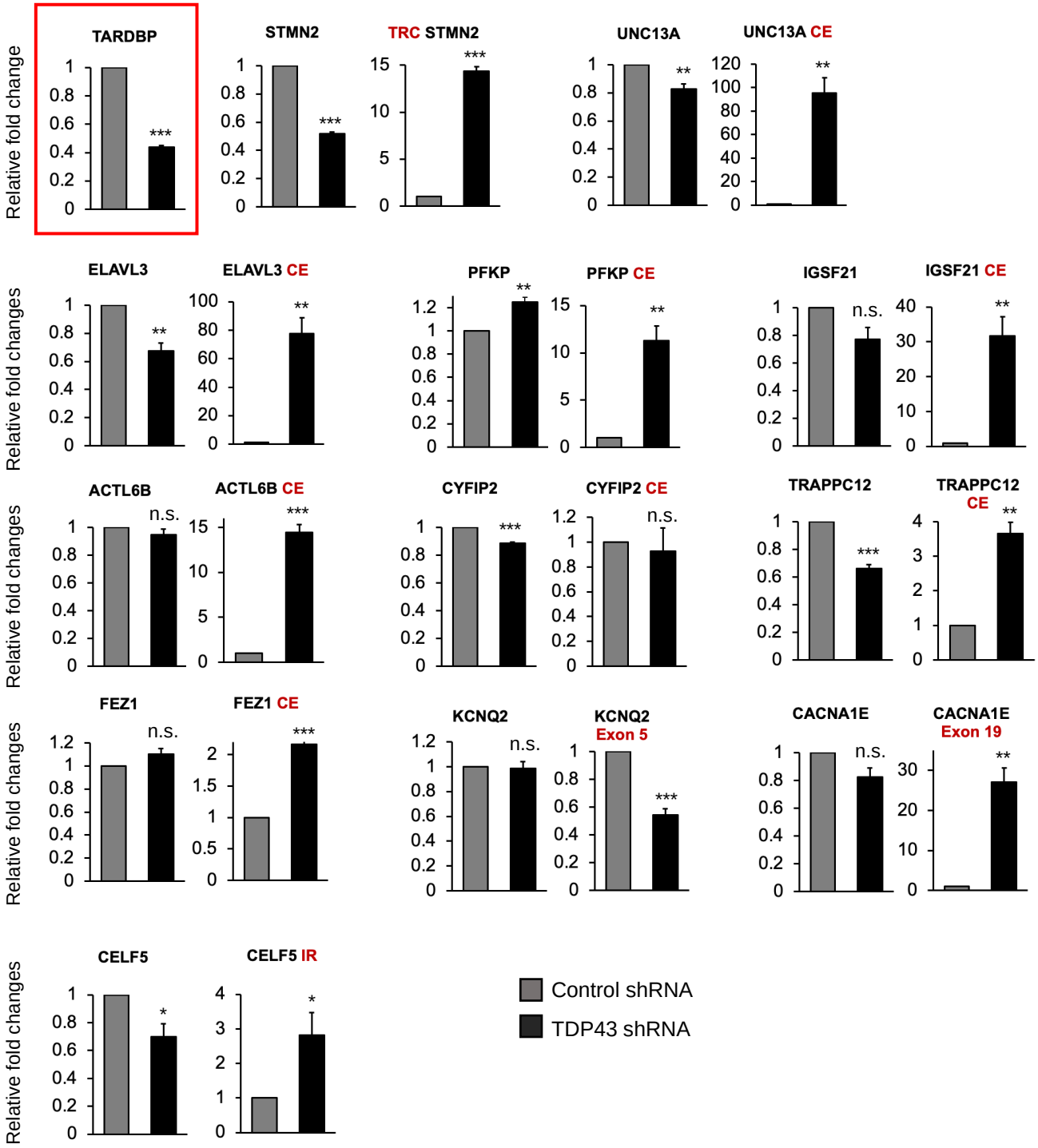

Supplementary Figure 6. (Related to Figure 2)

RT-qPCR showing alternative splicing errors in unedited iPSC MNs, 10 days post-addition of shRNAs targeting TDP43, or controls. The chart showing successful TDP43 knockdown is highlighted in red. Error bars show SEM. CE = cryptic exon, TRC = truncated, IR = intron retention. N = 3 independent differentiations.

* indicates $p < 0.05$, ** indicates $p < 0.01$, *** indicates $p < 0.001$.

Supplementary Figure 7

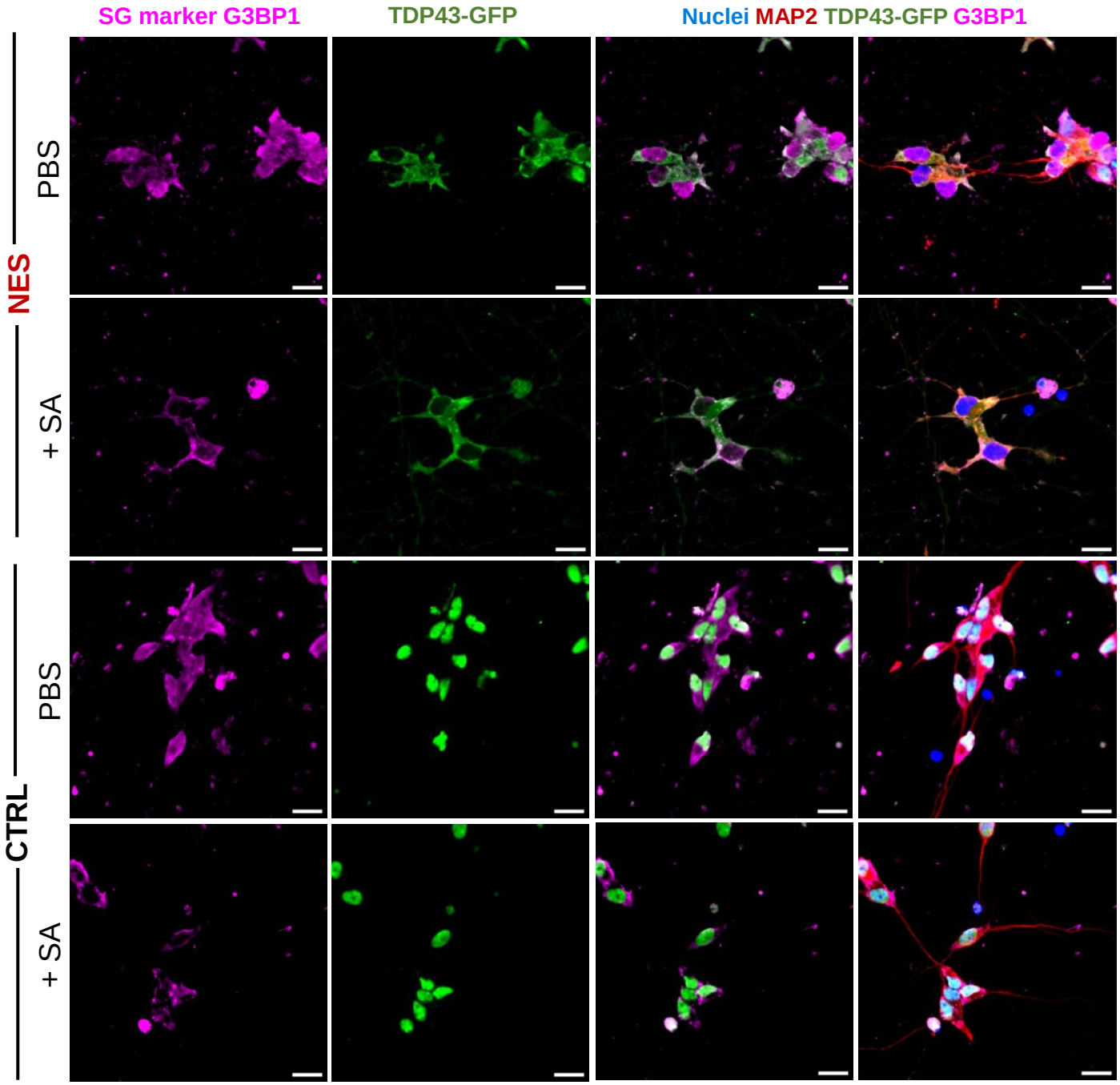

Supplementary figure 7 (related to figure 3): TDP43-GFP mislocalization is distinct from stress granule formation.

Representative images of TDP43-GFP-NES or –CRTL lines with and without SA exposure (500 µM for 60 minutes), 3 days in Dox (1 ug/mL). G3BP1+ Stress granules were observed only with SA treatment. Cytoplasmic TDP43-GFP puncta in the NES line do not fully co-localize with stress granules.

Cells were fixed and stained at day 23. Scale bar = 20 µm.

Supplementary Figure 8

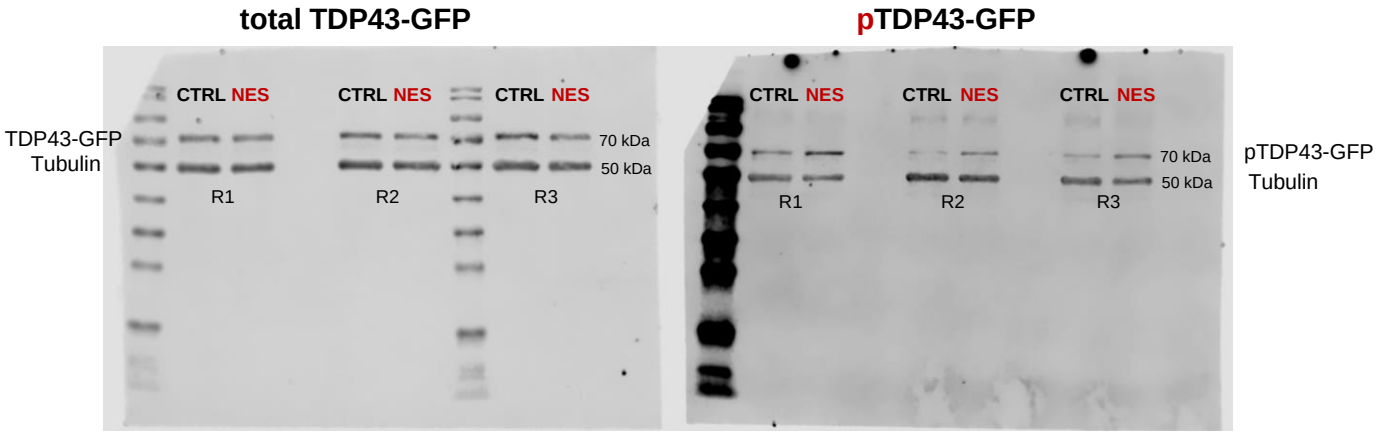

Uncropped Western Blots

Supplementary figure 8: (related to figure 3) Uncropped western blots for total and phosphorylated TDP43.
Protein from TDP43-GFP-CTRL or –NES MNs was collected day 40 (20 days post-Dox, 1 ug/mL) and stained for total TDP43 and phosphorylated TDP43 (pTDP43-GFP). Alpha-tubulin was used as a loading control. Three replicates from independent differentiations are shown.

Supplementary Figure 9

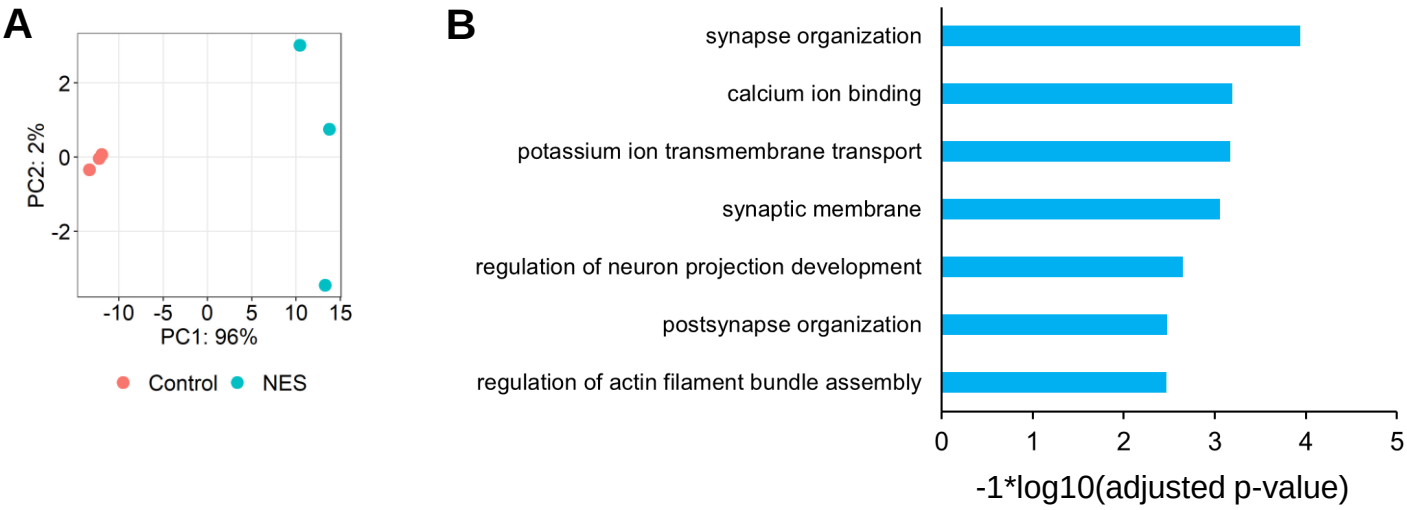

Supplementary figure 9: (related to figure 3) Transcriptomic analysis of day 40 MNs using the Dox inducible TDP43 model.
(A) PCA plot using the top 500 most variable genes. Control: MNs expressing the control nanobody, NES: MNs expressing the NES nanobody.

(B) GO enrichment analysis of 494 genes mis-spliced in the NES MNs compared to Control MNs. Splicing changes were detected using leafcutter at an adjusted p-value < 0.01 and delta-Psi > 0.1.

Supplementary Figure 10

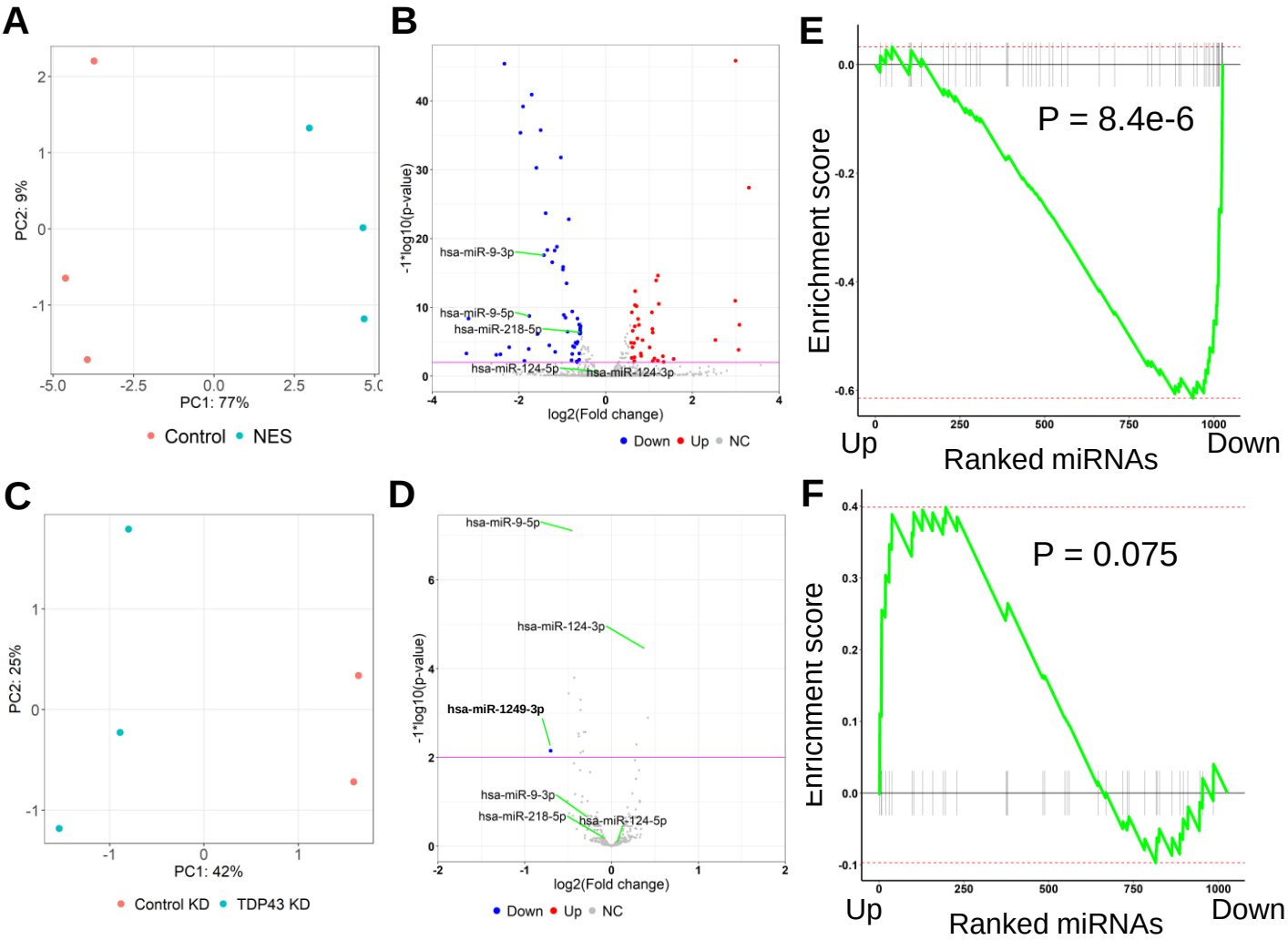

Supplementary figure 10: MicroRNA dysregulation in MNs due to TDP43 mislocalization or knockdown.

(A) Principal component analysis of microRNA (miR) counts for the TDP43-GFP-Control and TDP43-GFP-NES MNs.

(B) Volcano plot displaying miRs differentially expressed due to TDP43 mislocalization. Red: upregulated miRs, Blue: downregulated miRs, NC: No Change. Horizontal line denotes a p-value threshold of 0.01.

(C) Principal component analysis of miR counts for unedited healthy iPSC MNs transduced with TDP43 or control shRNAs.

(D) Volcano plot displaying miRs differentially expressed due to TDP43 knockdown. Blue: downregulated miRs, NC: No Change. Horizontal line denotes a p-value threshold of 0.01. Only miR-1249-3p was deemed differentially regulated at the thresholds used.

(E, F) Gene-set enrichment analysis plots displaying overlap of differentially expressed miRs due to TDP43 mislocalization or knockdown. miRs differentially expressed in the TDP43 knockdown samples were ranked from most upregulated to the most downregulated. **E**: Gene set used for the GSEA include miRs downregulated due to TDP43 mislocalization, **F:** Gene set used for the GSEA include miRs upregulated due to TDP43 mislocalization**.**

Supplementary Table 1

Target	AS event	AS event loc.	Forward sequence	Reverse sequence
UNC13A	canonical transcript		GGACGTGTGGTACAACCTGG	GTGTACTGGACATGGTACGGG
UNC13A-CE	cryptic exon	intron 19	TGGATGGAGAGATGGAACCT	GGGCTGTCTCATCGTAGTAAAC
STMN2	canonical transcript		AGCTGTCCATGCTGTCACTG	GGTGGCTTCAAGATCAGCTC
STMN2 trunc	Cryptic exon	intron 1	GGACTCGGCAGAAGACCTTC	GCAGGCTGTCTGTCTCTCTC
ELAVL3	canonical transcript		TGCAGACAAAGCCATCAACACCC	GCTGACGTACAGGTTAGCATCC
ELAVL3-CE	cryptic exon	intron 3	CCTGCTCTGAGGGATTGAGT	GTACAGGTTAGCATCCCGGA
PFKP	canonical transcript		AGGCAGTCATCGCCTTGCTAGA	ATCGCCTTCTGCACATCCTGAG
PFKP-CE	cryptic exon	intron 3	CTACCAGGGCATGGTGGA	GGAGAGTGTCTCCAGCATCC
ACTL6B	canonical transcript		CTTCCACATCGACACCAATGCC	CAGGTTTGGCTCAGACTTGACG
ACTL6B-CE	cryptic exon	intron 4	CCTGGATCACACCTACAGCA	ACCCAGGAGTTCGAAACTAGC
IGSF21	canonical transcript		GTCTGGAGGAAAACCAGCAC	TCTTGGTGTCATCCAGGTCA
IGSF21-CE	cryptic exon	intron 2	GCCTGCAGGAGGTGTTTATG	CTCTCGCTTGCGGTAGTTCT
CYFIP2	canonical transcript		ATGCCCTGGATTCTAACGGACC	CTTGGTCAGAGCATAGTAGGCG
CYFIP2-CE	cryptic exon	intron 25	CTCCAAGGAACCATTCTCCA	TGAGATTTCTTTCAGGGCTCA
FEZ1	canonical transcript		CCACTGGTGAGTCTGGATGA	TGGATCCCTCCAGTCTTCTG
FEZ1-CE	cryptic exon	intron 1	TGGAGATGTGGGATGATGG	AGGGTCGAAGGTCCTCAAAC
CELF5	canonical transcript		CACCTACTGTGCCAGGGATT	ACTGTCCGCAGGCTTCAC
CELF5-IR	intron retention	intron 5	CGTGAAGTTCTCCTCCCACA	CATCTGCACACACTCACACG
CACNA1E	canonical transcript		CCATTGTCCATCACAACCAG	CCATGCCATACATCTTCAGG
CACNA1E-E19	exon 15 inclusion	exon 19	GAGGCCTTCAACCAGAAACA	CGACATGTGGTGTCTTCTCC
KCNQ2	canonical transcript		AGTACCCCCAGACCTGGAAC	TTCCGCCTCTTCTCAAAGTG
KCNQ2-E5	exon 5 exclusion	exon 5	ACGTCTTTGCCACATCTGC	CCCCTTCTCTGCCAAGTACA
TRAPPC12	canonical transcript		TCGTGGACAAGGAGAACCTCAC	GGACTTGTCTCTTTGCTGCAGC
TRAPPC12-CE	cryptic exon	intron 7	ATGTGCAGCCCAAGTCAAG	TTGCCATGGAGTACATCACC

Supplementary table 1: Table of qPCR primers. AS = Alternative splicing.

Supplementary Table 2

Immunofluorescence antibodies:

Antibody	Species	Dilution	Source
GFP	Goat	1:1,000	NB100-1770 (Novus/Bio-techne)
MAP2	Chicken	1:10,000-16,000	GTX82661 (GeneTex)
TDP43	Rabbit	1:800	10782-2-AP (Proteintech)
Cleaved Caspase 3	Rabbit	1:400	9664L (Cell Signalling)
Neurofilament-M	Mouse	1:1,000	Mab1621 (Merck)
ISLET-1	Rabbit	1:500	Ab109517 (Abcam)
V5 tag	Mouse	1:1,000	MA5-15253 (Invitrogen)
G3BP1	Rabbit	1:1,000	13057-2-AP (Proteintech)

Western blotting Antibodies:

Antibody	Species	dilution	Source
TDP43	Rabbit	1:1,000	10782-2-AP (ProteinTech)
Phospho-TDP43	Mouse	1:1,000	TIP-PTD-M01A (Cosmo Bio)
Alpha-tubulin	Mouse	1:1,000	AB7291 (Abcam)
Alpha-tubulin	Rabbit	1;1,000	AB4074 (Abcam)
IRDye® 680RD anti-mouse	Goat	1:5,000	926-68070 (Li-Cor)
IRDye® 800CW anti-rabbit	Goat	1:5,000	926-32211 (Li-Cor)

Supplementary table 2: antibodies used for immunofluorescence and western blotting